Bollettino di Geofisica Teorica ed Applicata Vol. 62, n. 2, pp. 203-230; June 2021
DOI 10.4430/bgta0309

Detection and location analysis of the Minerbio integrated seismic network (Bologna, northern Italy)

S. Carannante, E. D'Alema, P. Augliera and G. Franceschina
Istituto Nazionale di Geofisica e Vulcanologia, Milano, Italy

(Received: 2 July 2019; accepted: 1 December 2019)

ABSTRACT Detection analyses are necessary to plan microseismic networks for use in the monitoring of anthropic activities. In 2014, the Italian Ministry of Economic Development (MiSE) issued guidelines for the monitoring of microseismic activity, ground deformations, and reservoir pore pressure. In 2016, the Istituto Nazionale di Geofisica e Vulcanologia (INGV) was commissioned to carry out specific investigations, aimed at assessing the guidelines applicability at the pilot site of the gas storage concession "Minerbio Stoccaggio" (Bologna). In this work, we present an overview of detection analysis, performed by the INGV team, during the experimental phase of the above mentioned guidelines. Measurements of ambient seismic noise, performed from 1 January 2018 to 31 March 2019, were used to assess detection thresholds of different configurations of the Minerbio Integrated Seismic Network (MISN). Detection analysis is particularly relevant for the Inner Domain of Detection (IDD), the crustal volume centred on the reservoir, within which it is vital to ensure the highest network performance. The results obtained in this work, validated through data recorded by the MISN during the analysed period, show that in the worst noise conditions observable in the area, the final configuration of the MISN enables localising $M_L \geq 1.0$ events occurring in the whole IDD, in line with the monitoring requirements prescribed by the guidelines.

Key words: induced seismicity, detection threshold, seismic ambient noise, microseismic monitoring.

1. Introduction

The Minerbio Integrated Seismic Network (MISN) has been installed in the area of the natural gas storage concession "Minerbio Stoccaggio", assigned by the Italian Ministry of Economic Development (MiSE) to Stogit (Snam group), Italy's leading operator in the storage of natural gas. The monitoring of this area, as regards seismicity, ground deformations, and reservoir pressures, is carried out by Stogit (hereinafter referred to as "Concessionaire") with the aim of verifying the safety conditions of the storage facility. In particular, since 1979, seismic monitoring was carried out by a microseismic network, which during this forty-year operational period had different configurations and adopted different acquisition systems. Data acquisition in continuous mode started in 2015 with 3 surface stations and 1 borehole station (100 m depth). Stations are located at the surface projection of the reservoir, represented by a series of sandy levels of turbiditic nature belonging to the Porto Garibaldi Formation (Plio-Pleistocene) with a thickness of about 80 m, separated by clayey levels of limited thickness. The reservoir, located at about 1300 m depth,

extends for a total area of about 8 km^2 and belongs to the category of the depleted natural gas or oil fields, which were used in the past for hydrocarbon production and, then, converted into underground storage sites.

In 2016, in the framework of an operating protocol signed by MiSE, Emilia Romagna Region and Stogit, concerning the concession "Minerbio Stoccaggio", the Istituto Nazionale di Geofisica e Vulcanologia (INGV) was commissioned to carry out specific investigations aimed at assessing the applicability of the guidelines for monitoring anthropic activities issued by MiSE in 2014 (MiSE - DGS - UNMIG, 2014, hereinafter referred to as ILG). The ILG aims to establish protocols for microseismic, ground deformation, and pore pressure monitoring, and represents the first action promoted by MiSE towards keeping the safety standards for monitoring mining subsurface activities. The guidelines collect technical specifications on monitoring networks, decision-making framework and related procedures in the field of underground fluid exploitation and storage activities, and plan to be re-evaluated two years after their first experimental application on pilot test sites (Morelli *et al*., 2018).

Worldwide, due to the growth of various underground industrial activities in highly populated regions, the number of events suspected (or considered) as "man-made" earthquakes has increased in recent years (Wilson *et al*., 2017). A review of anthropogenic seismicity in Italy can be found in Braun *et al*. (2018). In this context, microseismic monitoring plays a fundamental role in the detection and management of induced seismicity related to human activities such as: hydrocarbon extraction and natural gas storage operations, hydrofracking, geothermal energy exploitation, mining operations, CO_2 sequestration, and water impoundment (Kraft and Deichmann, 2014; Edwards *et al*., 2015; Priolo *et al*., 2015; Grigoli *et al*., 2017).

In principle, monitoring should begin before the start of human activities in order to assess the background level of natural seismicity of a region. During the operational period, the monitoring aims to detect changes in the parameters monitored, highlighting their possible correlation with the ongoing activity. Monitoring should also allow to track the evolution of seismicity in order to undertake mitigation actions, needed to bring the measured parameters to the previously assessed background values. Improving detection capabilities of microseismic networks committed to the monitoring of these human activities is a necessary condition to achieve this goal. However, technical specifications of a microseismic network designed to guarantee the required monitoring conditions are not yet standardised and, in recent years, various methods of network design for microseismic monitoring applications have been proposed (Grigoli *et al*., 2017).

In the literature, the detection capability is often expressed as a magnitude of completeness, *Mc*, defined as the lowest magnitude of events that a network is able to record reliably and completely (Evernden, 1969). *Mc* is a four-dimensional function of space and time. However, for statistical analysis of earthquakes, completeness levels are generally evaluated as average values over space and time using only information from earthquake catalogues. *Mc* is, then, often estimated as the deviation point from the Gutenberg - Richter line (*b*-value fit) in the cumulative frequency-magnitude distribution (Wiemer and Wyss, 2000; Cao and Gao, 2002; Woessner and Wiemer, 2005; Amorese, 2007). A different method to evaluate completeness levels was introduced by Schorlemmer and Woessner (2008), through the computation of the so-called probability-based magnitude of completeness (PMC). The method uses information about: on- and off-times of each station in the network, phase picks of earthquakes recorded by each station, and attenuation relation used for magnitude determination. Schorlemmer *et al*. (2010) computed PMC for the

Italian Seismic Network (ISN), concluding that in 2010 the network was complete at $M = 2.9$ for the entire Italian territory excluding the islands of Sardinia, Pantelleria, and Lampedusa.

For network design or network implementation purposes, detection thresholds can be evaluated through ground motion simulations. Information about seismicity is replaced by considering synthetic time series and corresponding spectra, associated with rupture models of earthquakes. Synthetic spectra are, then, compared with the noise level recorded at the single stations. Afterwards, the detection of an event occurring within a crustal volume, which includes the monitored area, is declared when the earthquake spectrum exceeds the noise level at a sufficiently large number of stations to accurately locate the event. Event sizes are specified in terms of seismic moment, M_0, and the network performance is, then, evaluated in terms of moment magnitude, M_W. Finally, detection thresholds, M_W^{det}, and location thresholds, M_W^{loc}, are mapped over the source region (Vassallo *et al*., 2012; Stabile *et al*., 2013), together with the maps of the spatial and temporal errors expected on event location (D'Alessandro *et al*., 2011; Stabile *et al*., 2013; Tramelli *et al*., 2013; Kwiatek and Ben-Zion, 2016).

In this paper, we describe the analysis performed by INGV in order to establish detection and location thresholds of the different configurations adopted during a two-year experiment by the microseismic network installed in the area of the storage concession "Minerbio Stoccaggio". According to the ILG, the network was integrated with stations of the ISN. Thresholds were established in terms of local magnitude, M_L, through numerical simulations of seismic point sources whose parameters were calibrated by using earthquakes data recorded in this period in the area. Measures of the Power Spectral Density (PSD) of ambient seismic noise, performed at all installation sites during at least one year monitoring, were employed to characterise the average levels of anthropic disturbance, necessary to evaluate detection thresholds. In order to validate the simulated location thresholds with real data, we also present a preliminary analysis of data recorded by the network from 1 January 2018 to 31 March 2019.

2. Geological framework and monitoring area

The storage concession "Minerbio Stoccaggio" covers a 69 km^2 area, in a region characterised by intense anthropic activity, both as regards production activities and the presence of important communication routes. The gas storage involves six municipalities, all of which are located in the province of Bologna: Minerbio, Malalbergo, Bentivoglio, Granarolo dell'Emilia, Budrio, and Baricella. 65% of the area of the above mentioned concession is located in the municipality of Minerbio, which also hosts the whole surface projection of the reservoir. The depleted gas field lies within the westernmost side of the Romagna Fold system, one of the Quaternary compressive structures that characterise the external part of northern Apennines (Burrato *et al*., 2003; Boccaletti *et al*., 2011). This chain is formed by the superposition of different tectonic units, deformed and detached from its own base, and shifted from very different paleogeographic domains, through a long process started in the Oligocene. The current configuration of the northern Apennines is the result of intense tectonic phases begun in the late Miocene (together with the opening of the Tyrrhenian basin), while the current structural setting of the "Ferrarese - Romagnola" ridge, which includes the Romagna Fold system, is the result of the Apennine compression occurring in the Pliocene-Pleistocene.

During this period, the region underwent strong tectonic activity that led to the deformation, lifting, inclination, and faulting of the area that hosts the reservoir. Moreover, the deposition of turbiditic sediments led to the genesis of the formations of Porto Corsini and Porto Garibaldi on a large part of the foredeep-foreland system. During the Upper Pliocene - Pleistocene, another tectonic event completed the structuring of the Ferrara Fold system and led to the lifting and tilt of the current area of Bologna (Ghielmi *et al*., 2013). Turbiditic sediments, belonging to the Porto Garibaldi formation observed in this area, also host the gas storage reservoir of Minerbio. The original gas-water contact (GWC) was found at 1370 m depth and extends for a total area of about 8 km^2. Above this level, 4 main sandy bodies with 3 interposed clayey layers of limited thickness, constitute the natural seat of the gas reservoir. The total thickness of the deposit is about 80 m. Geological confinement is guaranteed by the clayey-silty facies of the upper member of the Argille del Santerno formation, covering the whole area of the reservoir with an average thickness of about 120 m, and which constitute a continuous sealing. We adopt the GWC level as a reference, in order to define the crustal volumes involved in the monitoring activity (Fig. 1).

According to the ILG, we defined two different crustal volumes of earthquake detection: the Inner Domain of Detection (IDD) and the Extended Domain of Detection (EDD). The IDD is defined as the crustal volume within which the monitoring network must reach the highest detection capability, to allow the use of the most advanced techniques for location of earthquakes and the reconstruction of seismic velocity models and, if data are adequate, to track a possible migration of seismicity. The ILG require defining the IDD by extending horizontally the area corresponding to the surface projection of the reservoir, and by considering the maximum depth of the reservoir as a starting point in order to define the bottom of the monitored volume. For storage activities, the ILG prescriptions require that IDD is the volume that includes the mineralised area (reservoir used for storage), as defined by the geological study, and extends to a 2-3 km wide neighbourhood around the reservoir, depending on the reservoir size (ILG).

Following the above mentioned criteria, we defined the IDD as a volume of 10×10×5 km^3 whose surface projection is centred on the central point of the surface projection of the GWC area (Fig. 1). According to the ILG, the EDD is defined as an extension of IDD, in order to better constrain monitoring and to help the interpretation of the recorded seismicity within the existing structural and geological background. We defined the EDD as a crustal volume of 22×22×11 km^3 centred on the surface projection of the centre of the GWC area (Fig. 1).

3. Implementation of the seismic network and assessment of ambient seismic noise levels of the area

The storage concession "Minerbio Stoccaggio" is located in a region where the stations of the ISN (ISN, 2006) allow reaching a minimum location threshold $M_L^{loc} = 2.0$, with a 50% probability to locate M_L 1.5 earthquakes (Schorlemmer *et al*., 2010). At present, in a 110×110 km^2 area centred on the surface projection of the reservoir, there are 13 stations of the ISN, equipped with the following instruments:

- one three-component broadband seismometer with flat response to velocity from 0.008 Hz (T = 120 s) to 80 Hz;

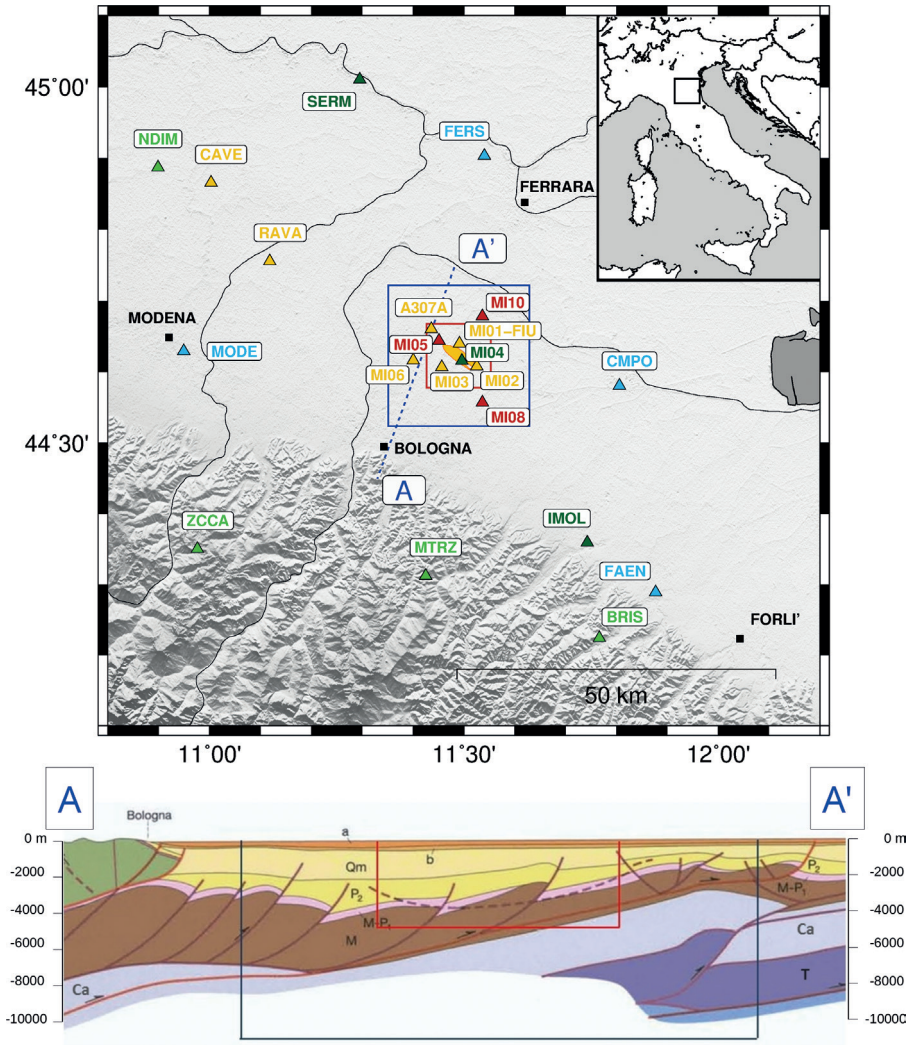

Fig. 1 - Upper panel: MISN and the crustal volumes involved in monitoring: IDD (red line) and EDD (blue line). Surface stations: velocimeters (yellow symbols); accelerometers (cyan symbols); double sensor stations (light green symbols). Borehole stations: velocimeters (red symbols). Double sensor stations equipped with surface accelerometer and borehole velocimeter (dark green symbols). The yellow area at the centre of the figure marks the surface projection of the GWC surface. Lower panel: main structural stratigraphic features along section A - A', drawn on the upper panel (modified from Boccaletti *et al.*, 2011). Stratigraphy: a - Middle Pleistocene-Holocene; b - Middle Pleistocene; Qm - Lower Pleistocene; P2 - Middle-Upper Pliocene; M-P1 - Upper Messinian-Lower Pliocene; M - Miocene; Ca - Meso-Cenozoic carbonatic succession; T - Lower-Middle Triassic. Projections of the volumes IDD and EDD are marked with red and blue lines, respectively. Depths of IDD and EDD are 5.0 and 11.0 km, respectively.

- four three-component seismometers with flat response to velocity from 0.025 Hz (T = 40 s) to 40 Hz;
- two three-component seismometers with flat response to velocity from 0.2 Hz (T = 5 s) to 40 Hz;
- two three-component borehole seismometers with flat response to velocity from 1.0 Hz (T = 1 s) to 100 Hz;
- ten three-component accelerometers with flat response to acceleration up to 100 Hz, and full scale set at ±2 g.

Six stations are equipped with both velocity and acceleration sensors with a spacing of about 15 km. The well depths of borehole installations are 135 and 175 m. Except for FIU (station code in Table 1), the ISN stations are installed at distances ranging from about 25 to 55 km from the surface projection of the reservoir. Configuration and instrumental parameters of ISN stations are shown in Fig. 1 and Table 1, respectively. Since May 2015, the microseismic network managed by the Concessionaire in the storage area, has been equipped with a continuous mode acquisition system. This local network consisted of three surface stations (MI01, MI02, MI03) equipped with three-component short-period (T = 1 s) seismometers and one station equipped with a borehole three-component short-period (T = 1 s) seismometer and a surface accelerometer (MI04). Stations MI01 and FIU are co-located, and the well depth of the borehole installation is 100 m (Fig. 1 and Table 1). During the ILG experimentation phase, the microseismic network was implemented by installing three new three-component short-period (T = 1 s) borehole seismometers (well depths of 150 m) and one new three-component short-period (T = 1 s) surface seismometer. The network was completed in March 2018 (Fig. 1 and Table 1). According to the ILG, which prescribe inter-station distances of 3-5 km in the IDD, the station spacing of the microseismic network is 3.8 km. These stations are installed at distances ranging from 0.9 to 8.2 km from the surface projection of the centre of the GWC area, with 5 over 8 installations within the IDD. Finally, during almost the entire period of the ILG experimental phase (until April 2019), we were also able to exploit

Table 1 - Stations of the MISN. Net: MI (stations of the microseismic network managed by the Concessionaire), IV (stations of the ISN), Z3 (temporary stations of the AlpArray project). D: station distance measured from the surface projection of the centre of the reservoir; Azimuth: station azimuth measured with respect to the surface projection of the centre of the reservoir, MISN configurations: C1 (stations of the ISN), C2 (stations of the microseismic network installed before the experimental phase of the ILG), C3 (C1 + C2), C4 (stations of the microseismic network installed during the experimental phase of the ILG), C5 (C1 + C4), C6 (C5 + 2 AlpArray stations). Mean levels of velocity PSD of ambient seismic noise, in the frequency band 1-30 Hz: p10 (10th percentile of the PDF); p50 (50th percentile of the PDF); p90 (90th percentile of the PDF).

Net	Station Code	Lat. N (°)	Lon. E (°)	Elev. (m)	Depth (m)	Site	D (km)	Azimuth (°)	Digitizer	Sensor 1	Sensor 2	Start Time	Ending Time	C1	C2	C3	C4	C5	C6	p90-p50 (dB)	p50 (dB)	p50-p10 (dB)
MI	MI01	44.64014	11.49142	9	0	Minerbio - Fondo Fiumicello	1.9	3	Solgeo Dymas 24 M	LE3D-1S	_	2015-121	_		X	X	X	X	X	13.4	-141.9	10.0
MI	MI02	44.60820	11.52558	9	0	Minerbio - S.Martino in Soverzano	3.3	120	Solgeo Dymas 24 M	LE3D-1S	_	2015-121	_		X	X	X	X	X	11.2	-141.1	12.7
MI	MI03	44.60666	11.45678	15	0	Minerbio – Spettoleria	3.2	235	Solgeo Dymas 24 M	LE3D-1S-MKIII	_	2015-121	_		X	X	X	X	X	9.5	-144.0	9.7
MI	MI04	44.61596	11.49631	11	100	Minerbio – Tintoria	0.9	147	Solgeo Dymas 24 M	LE3D-BH	SARA SA10 2G	2016-118	2018-178		X		X			14.8	-155.0	7.8
										SARA SS10		2018-178	_			X		X	X			
MI	MI05	44.64411	11.45093	9	150	Bentivoglio – Saletto	3.9	307	Solgeo Dymas 24 M	SARA SS10	_	2018-103	_			X		X	X	4.7	-153.1	5.9
MI	MI06	44.61623	11.40021	17	0	Bentivolgio – Santa Maria in Duno	7.2	264	Solgeo Dymas 24 M	SARA S02	_	2018-103	_			X		X	X	8.6	-141.0	7.9
MI	MI08	44.55698	11.53678	18	150	Budrio – Riccardina	8.2	153	Solgeo Dymas 24 M	SARA SS10	_	2018-118	_			X		X	X	5.9	-158.7	6.6
MI	MI10	44.67853	11.53648	7	150	Malalbergo- Boschi	7.2	31	Solgeo Dymas 24 M	SARA SS10	_	2018-118	_			X		X	X	6.9	-160.0	6.0
IV	BRIS	44.22454	11.76657	260	0	Brisighella	49.5	153	GAIA2	TRILLIUM-40S	EPISENSOR-2G	2015-121	_	X			X	X	X	5.1	-157.9	9.3
IV	CAVE	44.86580	11.00310	18	0	Cavezzo	47.1	305	GAIA2	TRILLIUM-120S	_	2015-121	_	X			X	X	X	8.6	-139.3	9.9
IV	CMPO	44.58080	11.80560	2	0	Campotto Po	25.5	100	GAIA2	_	EPISENSOR-2G	2015-121	_	X			X	X	X	20.8	-141.0	5.8
IV	FAEN	44.28950	11.87700	41	0	Faenza	48.2	140	GAIA2	_	EPISENSOR-2G	2015-121	_	X			X	X	X	3.7	-132.5	6.0
IV	FERS	44.90350	11.54060	3	0	Ferrara	31.4	7	GAIA2	_	EPISENSOR-2G	2015-121	_	X			X	X	X	6.2	-133.3	5.3
IV	FIU	44.64014	11.49142	9	0	Minerbio - Fondo Fiumicello	1.9	3	GAIA2	LE3D-5S	_	2015-121	_	X						13.6	-141.5	10.3
IV	IMOL	44.35955	11.74248	27	175	Imola	35.5	145	GAIA2	LE3D-BH	EPISENSOR-2G	2015-121	_	X			X	X	X	10.0	-158.2	9.7
IV	MODE	44.62972	10.94917	41	0	Modena	42.9	271	GAIA2	_	EPISENSOR-2G	2015-121	_	X			X	X	X	5.2	-136.8	6.8
IV	MTRZ	44.31280	11.42480	570	0	Monterenzio	34.9	188	TRIDENT	TRILLIUM-40S	EPISENSOR-2G	2015-121	_	X			X	X	X	7.7	-154.3	7.0
IV	NDIM	44.88730	10.89870	19	0	Novi di Modena	55.3	302	GAIA2	TRILLIUM-40S	EPISENSOR-2G	2015-121	_	X			X	X	X	6.6	-130.7	10.5
IV	RAVA	44.75587	11.11880	15	0	Ravarino	32.9	297	GAIA2	LE3D-5S	_	2015-121	_	X			X	X	X	6.8	-140.2	9.4
IV	SERM	45.00997	11.29582	7	135	Sermide	45.7	340	GAIA2	LE3D-BH	EPISENSOR-2G	2015-121	_	X			X	X	X	4.0	-148.4	4.8
IV	ZCCA	44.35085	10.97650	700	0	Zocca	50.8	234	GAIA2	TRILLIUM-40S	EPISENSOR-2G	2015-121	_	X			X	X	X	7.3	-161.4	9.8
Z3	A307A	44.66076	11.43631	9	0	Bentivoglio	6.0	315	REFTEK130	TRILLIUM-120C	_	2015-121	2019-110						X	6.8	-145.6	6.1
Z3	A308A	44.58249	12.00568	-2	0	Longastrino	41.2	96	REFTEK130	TRILLIUM-120C	_	2015-121	2019-110						X	7.6	-138.0	13.7

data collected with two temporary stations of the AlpArray project (AlpArray Seismic Network, 2015). These stations (A307A and A308A) were equipped with three-component broadband seismometers with flat response to velocity from 0.008 Hz (T = 120 s) to 80 Hz. One of them was installed within the IDD at 6.0 km distance from the surface projection of the centre of the GWC area (Fig. 1 and Table 1).

Following prescriptions reported in the ILG, the MISN has been implemented by setting up a real-time acquisition system which stores in a unique archive, waveforms recorded through the microseismic network, managed by the Concessionaire, and waveforms recorded by stations of the regional networks operating in the area. Data are transmitted in continuous mode using different real-time technologies. Stations use commercial Transmission Control Protocol/Internet Protocol (TCP/IP) connections with dedicated cable or Universal Mobile Telecommunications System (UMTS) links. Raw data are acquired from the stations and, then, converted into MiniSEED format to be stored and processed. The real-time link and data archiving is performed through SeedLink protocol, developed within the SeisComp3 data acquisition system (https://www.seiscomp3.org/), which manages communications between stations and INGV acquisition servers located in the INGV acquisition centres of Milan or Rome, in case of ISN stations used in this work. As regards the microseismic network, the real-time link is performed between stations and the acquisition server managed by the Concessionaire. All data acquired in real-time at this server and at INGV servers which manage communications with ISN stations, are finally collected at the INGV server located in the acquisition centre of Milan.

Automatic signal quality control is performed by software PQLX (McNamara and Boaz, 2006, 2011), which evaluates in real-time stations baseline noise levels. The tool allows us to obtain the Power Spectral Densities (PSD) for investigations on the evolution of seismic noise. PSD curves are, then, arranged in order to compute Probability Density Functions (PDF), to be compared with the reference curves NHNM (New High Noise Model) and NLNM (New Low Noise Model) obtained by Peterson (1993). The software is based on the algorithm developed by McNamara and Buland (2004), which allows for robust estimations of baseline noise levels with no removal of earthquakes, system transients and data glitchers.

Fig. 2 shows PDF examples of ambient seismic noise measures, in terms of velocity PSD of the mean horizontal components recorded during the ILG experimentation phase at stations of the MISN. Stations installed on the Apennines and borehole stations installed in the Po Plain show comparable levels of ambient seismic noise (about -160 dB in the range of frequencies 1-30 Hz), 20 dB lower than the NHNM of Peterson (1993). For these stations, in this range of frequencies the noise variability can be quantified as ±7.5 dB around the median curves. In the range of frequencies 1-30 Hz, stations installed at the surface in the Po Plain show median levels of seismic noise of about -140 dB, comparable with the NHNM of Peterson (1993). These stations also show a noise variability of about ±8.0 dB around the median curves. Ambient seismic noise levels recorded with stations of the microseismic network confirm the above described behaviour, with mean values of PSD comparable with the NHNM curve of Peterson (1993) for surface installations, and 20 dB lower than the NHNM for the boreholes. On average, in the range of 1-30 Hz, ambient seismic noise levels recorded by stations of the microseismic network, are consistent with a decreasing rate of the PSD with depth, of about 0.1 dB/m (Franceschina *et al*., 2015). Fig. 3 shows the median curves of the PDF of noise recorded with all the stations of the microseismic network. Generally, borehole stations also show a lower variability of noise related to diurnal anthropic activities. Fig. 4

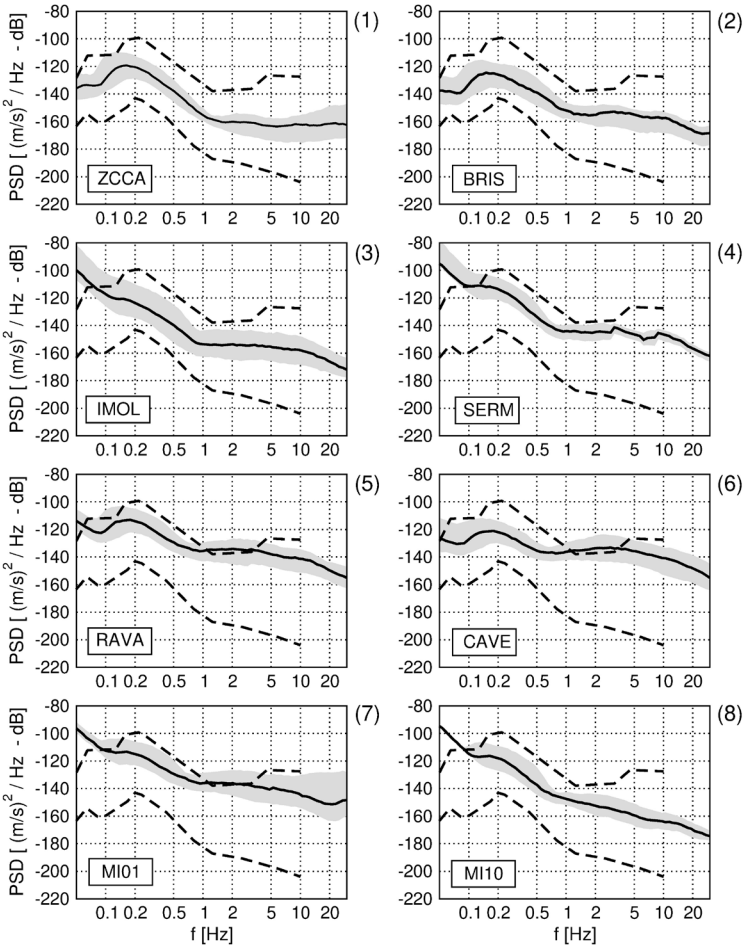

Fig. 2 - PDFs of velocity PSD of ambient seismic noise, measured during the ILG experimentation phase at some stations of the MISN. Median, 10th and 90th percentiles of the PDFs obtained with the mean horizontal components (continuous line and grey area), are compared with the NHNM and NLNM curves of Peterson (1993) (dashed lines). Panels 1 and 2: examples of surface stations of the ISN installed in the Apennines; panels 3 and 4: borehole stations of the ISN installed in the Po Plain; panels 5 and 6: examples of surface stations of the ISN installed in the Po Plain; panels 7 and 8: examples of stations of the microseismic network installed at the surface and in boreholes, respectively. Stations codes (see Table 1) are reported in each panel.

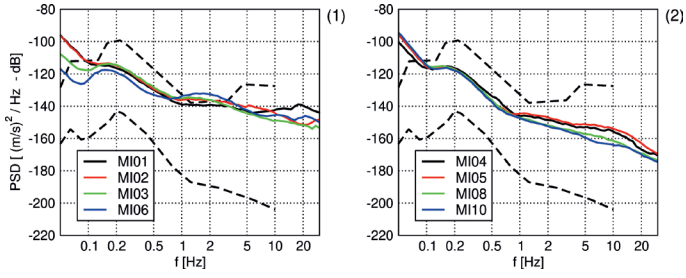

Fig. 3 - MISN: median PDF of velocity PSD of ambient seismic noise, measured during the ILG experimentation phase. Panel 1: surface stations; panel 2: borehole stations. Station codes (see Table 1) are reported in each panel. For each station, mean horizontal components are compared with the NHNM and NLNM curves of Peterson (1993) (dashed lines).

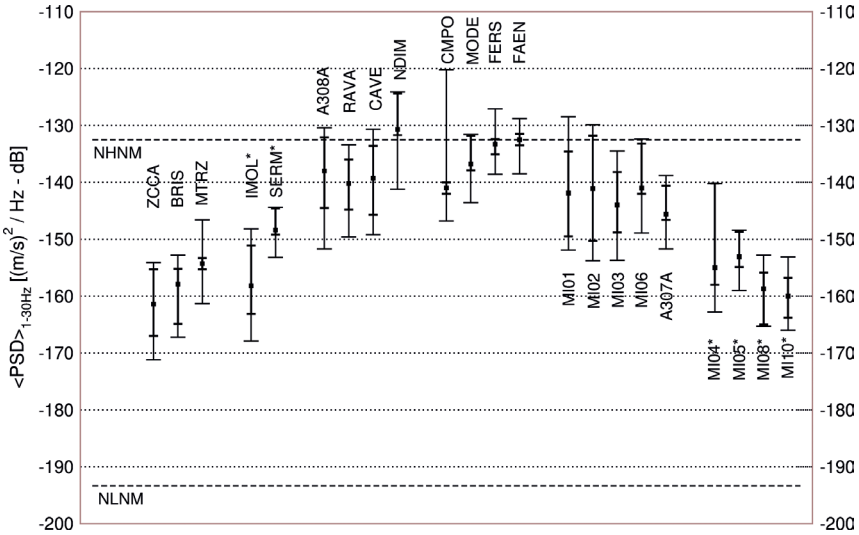

Fig. 4 - Mean PSD of ambient seismic noise measured at the MISN stations in the range of frequencies 1-30 Hz. Measurements performed with the mean horizontal components are compared with the NHNM and NLNM curves of Peterson (1993) (dashed lines). Thin vertical bars denote the variability of the PDF obtained in a 24-hour monitoring period, between the 10th and the 90th percentiles. Thick vertical bars denote the day-night variability of the PDF. Borehole stations are marked by an asterisk. ZCCA, BRIS, MTRZ: surface stations of the ISN installed in the Apennines; IMOL and SERM: borehole stations of the ISN installed in the Po Plain; A308A, RAVA, CAVE, and NDIM: AlpArray and ISN surface stations installed outside the EDD; CMPO, MODE, FERS, and FAEN: accelerometers installed outside the EDD; MI01, MI02, MI03, MI06, and A307A: surface stations installed within the EDD; MI04, MI05, MI08, and MI10: borehole stations installed within the EDD.

summarises the measurements of ambient seismic noise performed in the range of frequencies 1-30 Hz at all stations of the MISN. For each station, we considered the 10th, 50th, and 90th percentile curves of the PDF obtained with data collected in 24 hours of recording, and the median curves of the PDFs obtained by selecting day-time and night-time recordings. Mean values of the 10th, 50th, and 90th percentile curves, computed in the range of frequencies 1-30 Hz, were employed as reference measurements of noise for detection analysis (see Table 1).

To be able to manage detection and location scenarios obtained with different combinations of stations of the regional and microseismic networks, we introduce for MISN a total number of six network configurations (see Table 1). Indeed, until February 2018, the integrated network was composed of 4 stations of the microseismic network, 11 stations of the ISN and 2 AlpArray stations. Starting from March 2018, the microseismic network was completed with the installation of 4 new stations (3 of which are equipped with borehole sensors) and starting from May 2019 AlpArray stations were terminated. Configuration C5 refers to the present configuration of the MISN which does not include these temporary installations.

4. Detection analysis

4.1. Method

Detection analysis is performed by comparing the power spectrum of simulated earthquakes with the observed power spectrum of ambient seismic noise. Earthquakes of low-to-moderate magnitude

can be simulated through point source models and, as an example, the Brune (1970, 1971) model can be employed to reproduce the amplitude Fourier spectrum of the S waves, recorded at hypocentral distance R. The model neglects both finite fault effects and source directivity, and it is fully described by two parameters: seismic moment, M_0, related to the earthquake magnitude, and corner frequency, f_c, related to the linear dimension of the source. The seismic wave attenuation can be simulated by multiplying the source spectrum by a distance-dependent term, which takes into account anelastic absorption, scattering and geometrical spreading. In this study, we consider a R^{-1} dependence of geometrical spreading, a quality factor modelled by: $Q(f) = Q_0 f^n$, and a constant value of the high frequency decay parameter, k (Anderson and Hough, 1984). As a consequence, the velocity amplitude Fourier spectrum of S waves, recorded at hypocentral distance R, has been modelled as:

$$V(f) = \frac{C \bullet M_0}{R} \bullet \frac{2\pi f}{1 + \left(\frac{f}{f_c}\right)^2} \bullet exp\left(\frac{-\pi R f}{\beta Q(f)}\right) \bullet exp(-k\pi f) \qquad (1)$$

where β is the S-wave velocity, and the constant C is given by: $C = F_S R_{\theta\varphi}/4\pi\rho\beta^3$, with F_S, $R_{\theta\varphi}$, and ρ representing the free surface factor, the radiation pattern factor, and the density of the medium, respectively. We adopted β = 2.4 km/s and ρ = 2.6 g/cm^3, according to Carannante *et al*. (2015), and assumed $R_{\theta\varphi}$ = 0.63 for the RMS radiation pattern of S waves, Fs = 2 for surface stations and Fs = 1 for borehole stations. For any M_0 value, the corner frequency of the event is computed assuming a constant stress drop scaling $\Delta\sigma \div M_0 f_c^3$ with $\Delta\sigma$ = 2 MPa (Lay and Wallace, 1995). As we decided to express the final outcome of the work in terms of location thresholds of local magnitude, M_L, according to Hanks and Boore (1984) we relate the seismic moment to M_L by using the bilinear relation:

$$\begin{aligned} &\text{Log } M_0 = 1.5\, M_L + 9.0 && (M_L \geq 3.0) \\ &\text{Log } M_0 = 1.0\, M_L + 10.5 && (M_L < 3.0). \end{aligned} \qquad (2)$$

As regards the S-waves attenuation, recent studies performed in this region suggest a $Q(f) = 80\, f^{1.2}$ (Castro *et al*., 2013) and, from comparisons between simulated and recorded events, we inferred an average value of k = 60 ms for the area of the reservoir (Fig. 5).

In order to establish detection and location thresholds of the MISN, we used point source simulations of earthquakes characterised by different values of magnitude and distance, according to Eqs. 1 and 2. Simulations were carried out for seismic sources placed in 169 equally-spaced points of different regular grids, covering an area of 24×24 km^2, located in correspondence of the EDD, at depths ranging from 1.0 to 11.0 km. Grid levels of 1.5, 5.0, and 11.0 km coincide with the depth of the reservoir, the bottom of IDD and the bottom of EDD, respectively. We adopted seismic sources of M_L magnitude between -1.0 and 3.0 and considered a constant duration of 5 s in order to compute the earthquake power spectrum. For each site, earthquakes were considered to be detectable if the maximum value of the simulated earthquake spectrum exceeds by at least 14 dB the mean PSD of ambient noise recorded in the range of frequencies 1-30 Hz. This detection limit corresponds to a signal-to-noise ratio equal to 5.

We define as detection threshold, M_L^{det}, the minimum magnitude for which an earthquake can be recorded by at least one station of the network. The location threshold, $M_L^{loc}(N)$ is then the

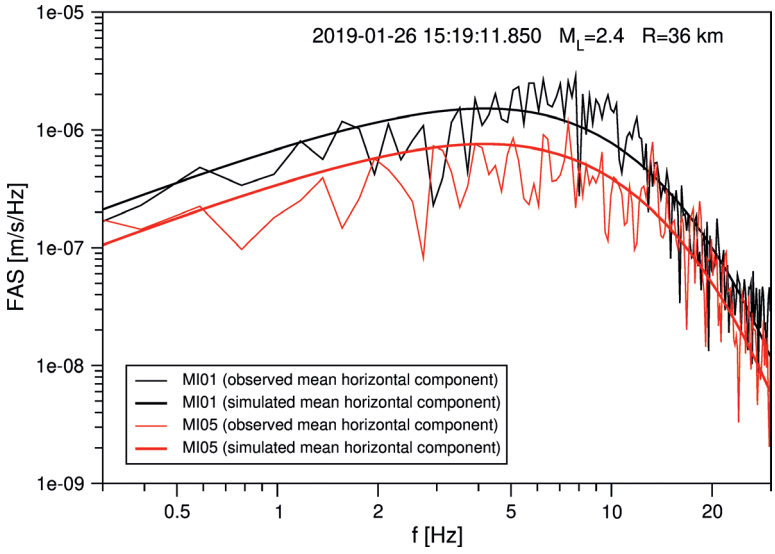

Fig. 5 - Examples of simulated and recorded Fourier amplitude spectra (FAS) of seismic events recorded by the microseismic network. Mean horizontal components of a M_L 2.4 event located at 36 km hypocentral distance, recorded by the surface station MI01 and by the borehole station MI05 (thin lines), are compared with the simulated ones (thick lines), in order to infer the simulation parameters.

minimum magnitude for which an earthquake can be detected by at least N (>1) stations of the network. Simulations are performed in three noise conditions, corresponding to the 10th, 50th, and 90th percentile of the PDF of the PSD of noise, illustrated in the previous section. In reference to Table 1, we consider the following MISN configurations:

C1. 13 stations of the ISN located in the range of distances 0-60 km from the reservoir;
C2. 4 stations of the microseismic network: MI01, MI02, MI03, MI04;
C3. configuration C1 + configuration C2 (without station FIU, co-located with MI01);
C4. 8 stations of the microseismic network: MI01, MI02, MI03, MI04, MI05, MI06, MI08, MI10;
C5. configuration C1 + configuration C4 (without station FIU, co-located with MI01);
C6. configuration C5 + 2 AlpArray stations: A307A and A308A.

Configuration C3 accomplishes the integration between the microseismic network and the ISN obtained before the improvement of the former ones. Configuration C5 achieves the same integration after the improvement of the microseismic network. It represents the present configuration of MISN and we consider the corresponding results as final results of the experimentation phase of the ILG. Configuration C6, which includes 2 temporary installations, is reported here in order to compare the final results with the network performance obtained during the experimentation phase.

4.2. Results

For each configuration and noise condition, detection maps have been produced for depth ranging between 1.0 and 11.0 km and location maps have been compiled for location thresholds $M_L^{loc}(N)$ with $N = 3$ and $N = 4$. As they depend on the detection of a certain number of stations, location threshold maps are characterised by a more homogeneous distribution with respect to detection threshold maps and, as expected, location thresholds increase with depth. Moreover, on the whole area considered in simulations, a general improvement of location thresholds moving from cases $N = 4$ to cases $N = 3$ can be observed (Fig. 6). In order to provide reliable location thresholds for the MISN, and especially considering the present, and probably future configuration of the network, in this work we present the case $N = 4$.

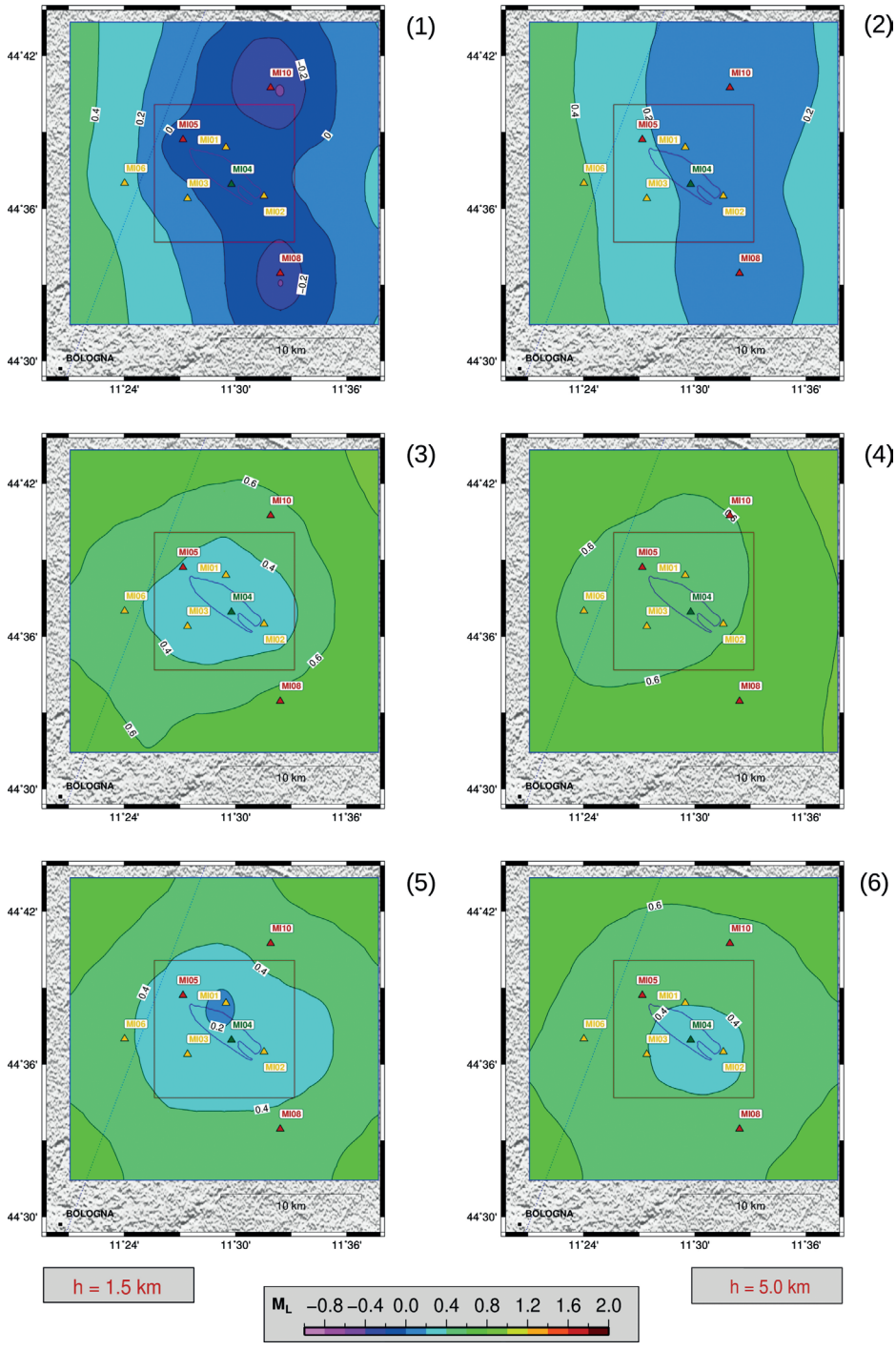

Fig. 6 - Detection and location maps, in terms of M_L magnitude, obtained with configuration C5 of the MISN (see above) for events located at 1.5 and 5.0 km depth (left and right panels, respectively). Assumed noise conditions correspond to the median of the measured PDF of ambient seismic noise. The IDD and EDD surface projections are marked with red and blue lines, respectively. The violet contour corresponds to the surface projection of the GWC area. Station symbols are as in Fig. 1. Panels 1 and 2: detection thresholds, M_L^{det}, for events located at 1.5 and 5.0 km depth, respectively; panels 3 and 4: location thresholds obtained with $N = 4$, $M_L^{loc}(4)$, for events located at 1.5 and 5.0 km depth, respectively; panels 5 and 6: location thresholds obtained with $N = 3$, $M_L^{loc}(3)$, for events located at 1.5 and 5.0 km depth, respectively.

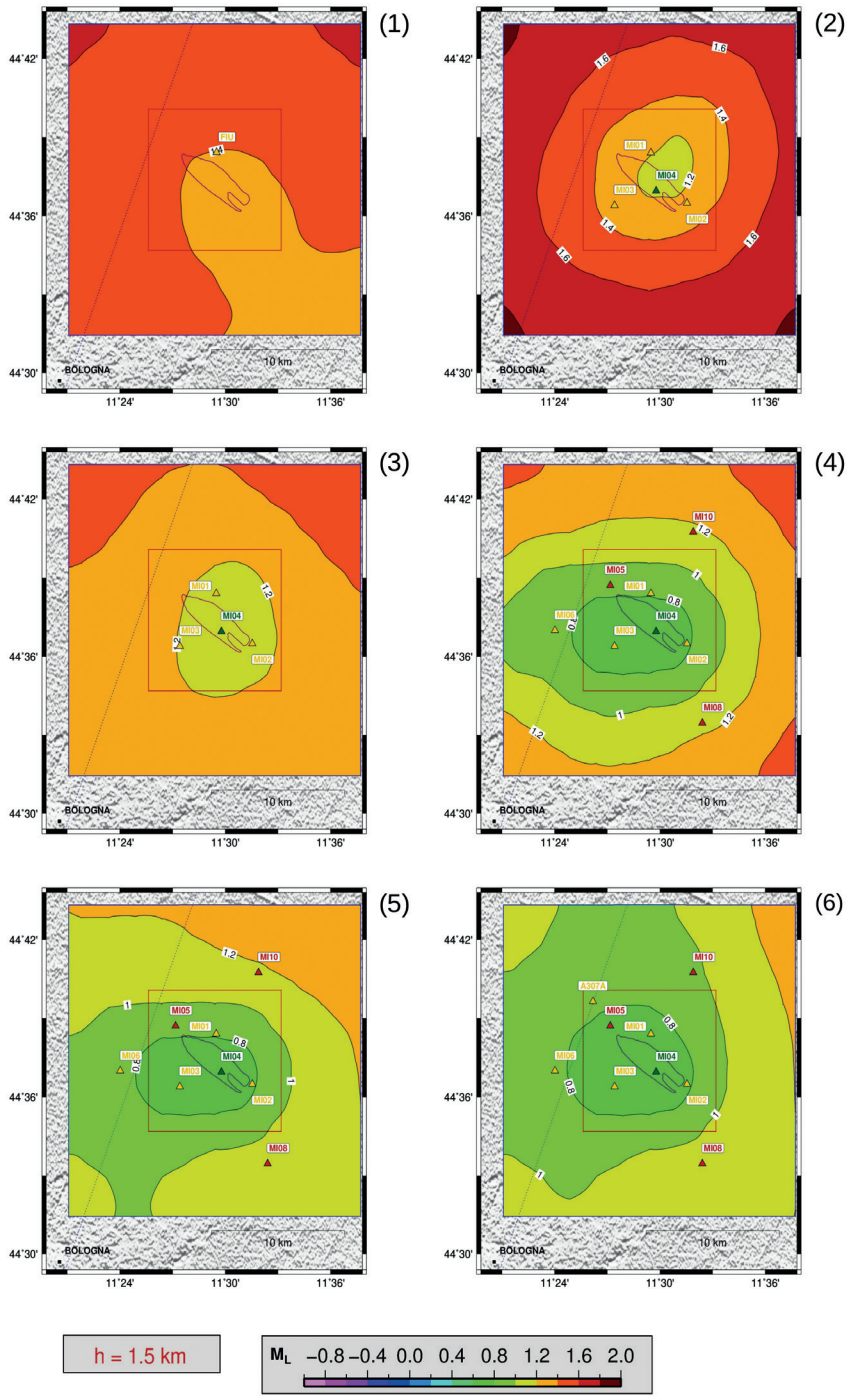

Fig. 7 - Location maps, in terms of M_L magnitude, obtained for $N = 4$ and with the different configurations considered for MISN, in case of seismic events located at the depth of the reservoir (1.5 km). Assumed noise conditions correspond to the 90th percentile of the measured PDF of ambient seismic noise. The IDD and EDD surface projections are marked as red and blue lines, respectively. The violet contour corresponds to the surface projection of the GWC area. Station symbols are as in Fig. 1. Configurations of the MISN: 1) stations of the ISN (configuration C1); 2) stations of the microseismic network installed before the experimental phase of the ILG (configuration C2); 3) configurations C1 + C2; 4) stations of the microseismic network installed during the experimental phase of the ILG (configuration C4); 5) configurations C1 + C4; 6) configuration C5 + 2 AlpArray stations.

Fig. 7 shows location thresholds $M_L^{loc}(4)$ obtained for sources located at 1.5 km depth in the case of noise conditions corresponding to the 90th percentile of the PDF of the PSD of measured ambient seismic noise. Comparison between configurations C1 and C2 shows that at the depth of the reservoir, stations of the ISN allow reaching a uniform location threshold of about 1.4 in the EDD, and that stations of the microseismic network installed in the area before the experimental phase of the ILG, allow obtaining a less uniform distribution of $M_L^{loc}(4)$, with values ranging from 1.1 to 1.4 in the IDD and from 1.4 to 1.8 in the EDD. By integrating the microseismic network with ISN stations, we obtain values of $M_L^{loc}(4)$ ranging from 1.1 to 1.3 in the IDD and from 1.3 to 1.5 in the EDD (see configuration C3). Configuration C4, obtained by adding 3 more borehole stations and 1 surface station to the original microseimic network, improves the results obtained with configuration C2. Within the IDD, $M_L^{loc}(4)$ values range between 0.7 and 1.0, while EDD is characterised by $M_L^{loc}(4)$ values ranging between 1.0 and 1.5. By integrating the implemented microseismic network with ISN stations, we obtain similar values of $M_L^{loc}(4)$ in the IDD and $M_L^{loc}(4)$ values ranging from 1.0 to 1.3 in the EDD (see configuration C5). Configuration C6 enables extending the area characterised by $M_L^{loc}(4) \leq 1.0$ to part of the EDD.

The comparisons between different configurations of the MISN, performed at the depth of the reservoir, can be extended down to the bottom of the EDD. Fig. 8 shows the mean values of $M_L^{loc}(4)$ computed at different depths within the IDD and in the part of the EDD not included in the IDD. Mean location thresholds are shown for noise conditions corresponding to 10th, 50th, and 90th percentiles of the PDF of the measured PSD of noise. The values of the curves corresponding to the highest noise conditions, obtained at the GWC level, are related to the maps shown in Fig. 7.

Results shown in Fig. 8 should be analysed by taking into account ILG prescriptions, which require $0 \leq M_L^{loc} \leq 1$ within the IDD. Considering unfavourable noise conditions (corresponding to the 90th percentile of the PDF), stations of the ISN allow locating earthquakes of $M_L = 1.5$ at all depths in both IDD and EDD (see configuration C1). By integrating the ISN with the stations of the microseismic network installed before the experimental phase of the ILG, in the same noise conditions we obtain an improvement of this threshold in the entire IDD. The integrated network allows locating events of magnitude 1.2 at all depths in this crustal volume (see configuration C3). The final configuration of the MISN, obtained after the installation of three new borehole instruments and one surface station within the EDD, further improves these thresholds, allowing to satisfy the ILG prescriptions. Indeed, through configuration C5, in the same noise conditions, the MISN is able to locate events of local magnitude in the range 0.8-1.0 occurring within the IDD. $M_L = 1.2$ is the corresponding threshold obtained for earthquakes located at all depths in the EDD. The comparison with results obtained through configuration C6 highlights that temporary AlpArray stations help improving the network performance, especially in the EDD.

Finally, it is worth mentioning that all of the above described results refer to particularly unfavourable conditions of ambient seismic noise. Noise variability can positively affect the network performance by decreasing M_L^{loc} values by about 0.5 and 1.0 units of magnitude, when noise conditions correspond to the 50th and to the 10th percentile of the PDF, respectively.

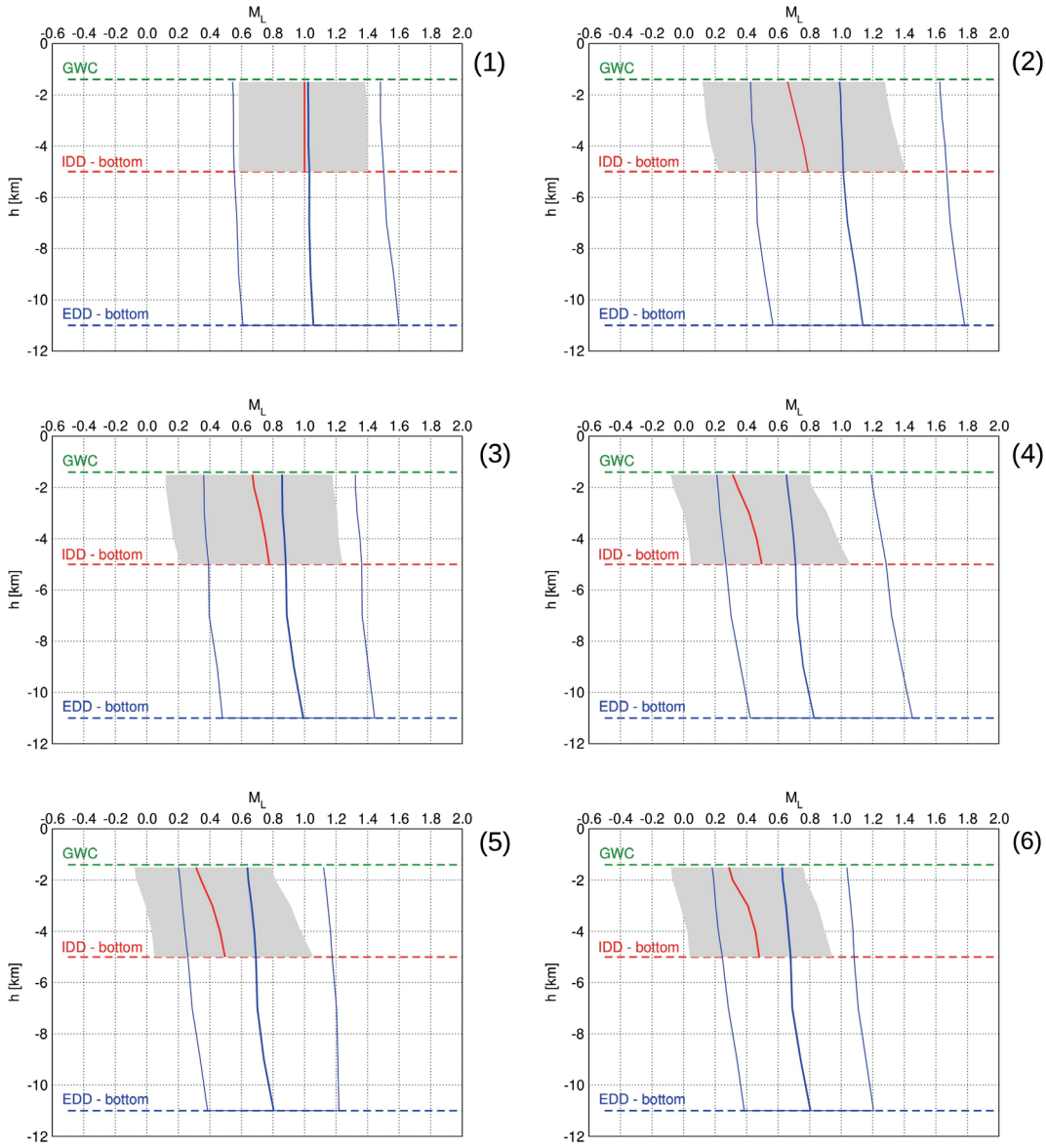

Fig. 8 - Mean values of location thresholds with respect to depth, obtained in the cases of Fig. 7. Red line: mean values obtained in the IDD in noise conditions corresponding to the median of the measured PDF of ambient seismic noise. Grey area: variability of the mean values obtained in the same crustal volume, for noise conditions ranging between the10th and the 90th percentile of the PDF of noise. Thick blue line: mean values obtained in the part of the EDD not included in IDD, in noise conditions corresponding to the median of the measured PDF of ambient seismic noise. Thin blue lines: variability of the mean values obtained in the same crustal volume, for noise conditions ranging between the 10th and the 90th percentile of the PDF of noise. The depths of the reservoir (GWC), of the bottom of IDD and of the bottom of EDD, are shown as green, red and blue dashed lines, respectively.

5. Local seismicity and validation of results

Since May 2015 and during the entire period of the ILG experimental phase (until April 2019), the MISN has continuously recorded local and regional seismicity. The recorded signals were

transmitted in real-time to the INGV data acquisition centre of Milan and processed in off-line mode in order to detect seismic events. We used software based on the STA/LTA (Short Time Average over Long Time Average) algorithm (Cattaneo *et al*., 2011), carefully calibrated in order to obtain high performances with small networks and very local seismicity. With the aim of obtaining a limited data set of transient signals consisting of events to be manually reviewed by an operator, we decided to apply trigger parameters that allowed identifying events with low signal-to-noise ratios. This choice, made to exploit the full advantage of the network detection capability, led to defining the following parameters: LTA = 30 s; STA = 1 s; threshold trigger (STA/LTA) = 3; search window for coincident triggers = 3 s; minimum number of stations for identification of an event = 3. The STA/LTA algorithm was carried out on band-pass filtered signals in the range 2-25 Hz, by considering only stations equipped with velocimeters. Applying the above criteria to all data recorded by the MISN in the period 1 January 2018 - 31 March 2019, enabled identifying 1127 transient signals. Afterwards, using the software package SacPicker (Spallarossa *et al*., 2011), each event was processed manually in order to identify seismic events. This second step allowed us to identify 224 earthquakes and classify the rest as transient signals caused by man-made disturbances or environmental noise. 198 of the 224 recognised seismic events, are included in the catalogue of the ISN (http://cnt.rm.ingv.it/ - last accessed 20 June 2019). Table 2 shows the bulletin of the earthquakes recorded by the MISN during the analysed period. Seismic events recorded at epicentral distances less than 50 km are shown in Fig. 9.

In order to classify the events in terms of their location and detection domains, we introduced the parameter Event-Type (see Table 2) and applied a first subdivision of the recorded

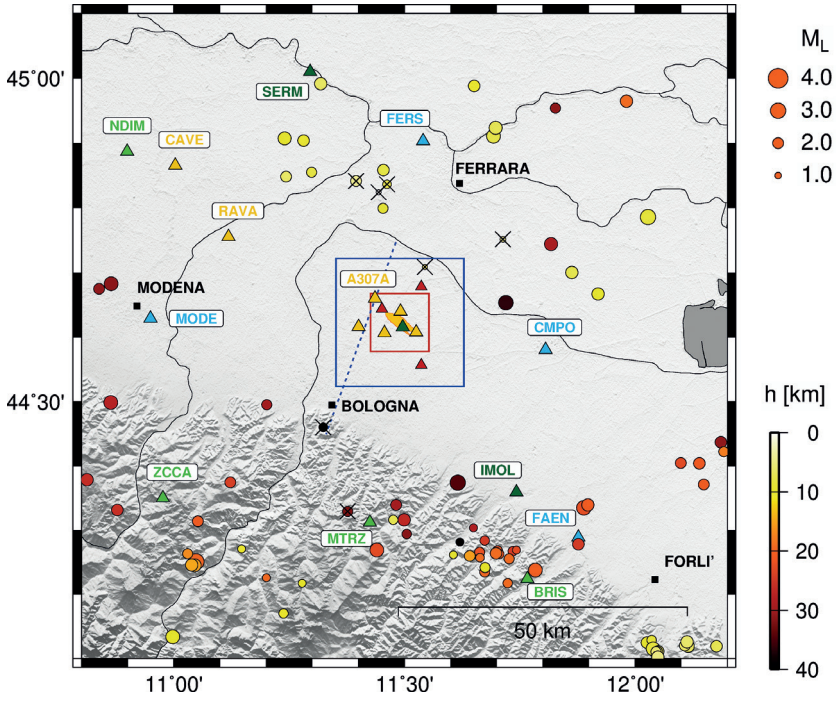

Fig. 9 - Seismicity recorded by the MISN in the period 1 January 2018 - 31 March 2019. Earthquake with epicentral distance less than 50 km are shown. Circle dimensions are proportional to the magnitude, colours indicate the event depth. Seismic events not included in the catalogue of the ISN are marked with crosses. Other symbols are as in Fig. 1.

Table 2 - Seismic events recorded by MISN in the period 1 January 2018 - 31 March 2019. Epicentral and hypocentral distances, *D* and *R*, respectively, with reference to the surface projection of the centre of the reservoir. Azimuth is computed with respect to the same point. NSP: number of pairs of P and S arrivals observed at the MISN stations. SN1 and SP1: code of the station showing the first P arrival and corresponding S-P interval in seconds. SN2-3: codes of the stations showing the second and the third P arrivals. ET: Event Type. Labels A and B denote events included and not-included in the ISN bulletin, respectively. Earthquakes labelled A are subdivided in: A0, A1, A2 or A3. A0: events with $R < 20$ km; A1: events with $20 \le R < 50$ km and with first arrival observed at one of the stations of the microseimic network; A2: events with $20 \le R < 50$ km and with first arrival not observed at one of the stations of the microseimic network; A3: events with $R \ge 50$ km. Earthquakes labelled B are subdivided in: B0, B1 or B2. B0: events with NSP < 4 and with first arrival observed at one of the stations of the microseimic network; B1: events with NSP ≥ 4 and with first arrival observed at one of the stations of the microseimic network; B2: events with NSP ≥ 4 and with first arrival not observed at one of the stations of the microseimic network. EC: Event Code. 1: seismic events localised within the IDD; 2: seismic events localised in the part of the EDD not include in the IDD; 3: seismic events localised outside the EDD. Location parameters of earthquakes with Event Types A1, A2 and A3 are taken from the catalogue of the ISN (http://cnt.rm.ingv.it/ - last accessed 20 June 2019).

Event ID	Origin Date	Origin Time	Latitude	Longitude	h [km]	M	M Type	D [km]	R [km]	NSP	SN1	SP1	SN2-3	ET	EC
20180104104747	2018-01-04	10:46:12.496	42.6190	19.8865	10.1	5.2	mb	712	712					A3	3
20180104201352	2018-01-04	20:13:35.250	44.3398	11.4818	29.7	2.0	ML	32	43	3	MTRZ	3.5	BRIS; MI02	A2	3
20180104201635	2018-01-04	20:16:29.090	44.3165	11.4993	26.7	2.3	ML	34	43	7	MTRZ	4.5	BRIS; MI02	A2	3
20180107024533	2018-01-07	02:45:15.640	44.1008	10.7908	11.7	2.3	ML	80	81					A3	3
20180110060353	2018-01-10	06:03:16.880	44.6852	10.0443	20.2	2.6	ML	115	116					A3	3
20180110230353	2018-01-10	23:03:31.050	44.6428	9.9217	24.4	2.6	ML	124	127					A3	3
20180111034856	2018-01-11	03:48:02.230	42.6412	13.2900	8.1	3.4	Mw	264	264					A3	3
20180113203927	2018-01-13	20:39:14.590	44.2947	11.5045	31.5	1.6	ML	37	48					A3	3
20180122113844	2018-01-22	11:38:13.560	44.1193	12.1768	7.2	2.2	ML	78	79					A3	3
20180122193430										3	IMOL	4.5	BRIS; MTRZ	B2	3
20180122212758	2018-01-22	21:27:51.080	44.3040	11.6492	28.4	1.3	ML	38	47	3	IMOL	3.3	BRIS; MTRZ	A2	3
20180131125326	2018-01-31	12:54:26.850	44.2180	11.7238	19.1	1.6	ML	49	52					A3	3
20180131225140	2018-01-31	22:51:34.120	44.3167	11.4757	7.3	1.7	ML	34	35	6	BRIS	5.0	MI02; MI03	A2	3
20180201010240	2018-02-01	01:02:35.850	44.6540	11.7202	36.4	2.8	ML	19	41	16	CMPO	5.0	MI02; MI04	A2	3
20180201014820	2018-02-01	01:47:32.660	47.1813	9.9928	11.4	3.8	ML	307	308					A3	3
20180203125423	2018-02-03	12:53:11.689	43.3178	16.8530	19.7	4.8	mb	453	454					A3	3
20180203131824	2018-02-03	13:18:11.600	44.9883	11.6507	10.7	2.1	ML	43	44	4	FERS	3.0	SERM; MI04	A2	3
20180204185807	2018-02-04	18:57:43.170	45.7087	10.6057	6.3	2.8	ML	140	140					A3	3
20180216122726	2018-02-16	12:27:11.420	44.4958	11.2018	29.7	1.9	ML	27	40	3	ZCCA	4.8	MTRZ; BRIS	A2	3
20180218040830	2018-02-18	04:07:49.920	44.2492	12.9372	24.6	2.0	ML	123	125	1	A308A	2.6		A2	3
20180219192940	2018-02-19	19:29:28.680	44.3752	11.1227	24.1	2.0	ML	40	47					A3	3
20180222043340	2018-02-22	04:33:25.040	44.4238	10.3633	22.5	3.4	ML	92	95					A3	3
20180225081705	2018-02-25	08:16:29.300	46.3763	12.5938	7.7	3.8	ML	213	213					A3	3
20180225155342	2018-02-25	15:53:04.860	46.3812	12.5987	7.0	3.6	ML	214	214					A3	3
20180301215246	2018-03-01	21:52:24.040	44.5290	10.2512	28.1	2.8	ML	99	103					A3	3
20180303201206										2	RAVA	2.6	CAVE	B2	3
20180304201652										6	FERS	3.1	A307A; MI01	B2	3
20180305215052	2018-03-05	21:50:35.890	43.9293	11.9653	6.8	3.7	Mw	86	86					A3	3
20180307201644	2018-03-07	20:15:15.400	39.3250	14.5012	379.0	4.4	ML	640	744					A3	3
20180323131224	2018-03-23	13:12:11.090	44.7442	11.8177	29.2	2.5	ML	29	41	5	A308A	3.9	FERS; MI02	A2	3
20180324210231	2018-03-24	21:01:58.680	44.0872	10.8188	10.9	2.4	ML	80	81					A3	3
20180326224343	2018-03-26	22:43:07.650	43.0467	12.8798	7.3	3.2	Mw	208	208					A3	3
20180326231116	2018-03-26	23:10:50.100	43.9740	11.8198	25.9	2.1	ML	77	81					A3	3
20180327171355										1	BRIS	3.2		B2	3
20180328033448	2018-03-28	03:34:33.730	43.9662	11.8147	26.9	2.3	ML	78	82					A3	3
20180328073721	2018-03-28	07:36:52.520	45.8702	11.8083	8.2	2.9	ML	141	141					A3	3

Table 2 - continued.

Event ID	Origin Date	Origin Time	Latitude	Longitude	h [km]	M	M Type	D [km]	R [km]	NSP	SN1	SP1	SN2-3	ET	EC
20180329163015	2018-03-29	16:31:10.060	44.2697	11.7428	22.8	1.4	ML	44	50					A3	3
20180329163016	2018-03-29	16:31:10.920	44.2697	11.7428	22.8	1.4	ML	44	50	1	BRIS	3.3		A2	3
20180329163016	2018-03-29	16:31:23.450	44.2678	11.7347	24.4	1.7	ML	44	50	1	BRIS	3.3		A2	3
20180329230119	2018-03-29	23:00:42.950	43.0322	11.5752	7.8	2.9	ML	177	177					A3	3
20180330001238	2018-03-30	00:11:29.070	46.9193	11.2387	11.3	2.7	ML	256	256					A3	3
20180331011928	2018-03-31	01:18:44.440	42.3528	13.4697	18.8	3.8	Mw	299	299					A3	3
20180401002222	2018-04-01	00:22:10.790	44.2558	11.7272	19.1	1.9	ML	45	49	11	BRIS	3.7	IMOL; FAEN	A2	3
20180401023217	2018-04-01	02:32:09.750	44.2605	11.6412	15.4	2.0	ML	43	44	10	BRIS	3.4	IMOL; FAEN	A2	3
20180401152223										5	MTRZ	6.8	ZCCA; MI03	B2	3
20180404022022	2018-04-04	02:19:45.510	43.0598	13.0312	7.8	3.9	ML	214	214					A3	3
20180404070324	2018-04-04	07:03:18.250	44.2633	11.7057	21.2	1.6	ML	44	48					A3	3
20180404184209	2018-04-04	18:41:28.710	43.0657	13.0298	8.1	3.9	ML	213	213					A3	3
20180405011507	2018-04-05	01:14:54.980	44.9917	11.3183	6.5	2.4	ML	43	44	12	SERM	2.1	FERS; CAVE	A2	3
20180409015814	2018-04-09	01:58:09.670	44.2643	11.6987	19.0	2.2	ML	43	47	13	BRIS	3.3	IMOL; FAEN	A2	3
20180410031130	2018-04-10	03:11:30.760	43.0687	13.0365	8.1	4.6	Mw	213	213					A3	3
20180411044223	2018-04-11	04:41:52.100	43.1340	10.8168	6.2	3.3	ML	174	174					A3	3
20180412022524	2018-04-12	02:23:59.780	47.0893	9.9788	8.2	2.9	ML	299	299					A3	3
20180421024724	2018-04-21	02:47:09.420	44.2682	11.7013	21.8	1.9	ML	43	48	4	BRIS	3.1	IMOL; MTRZ	A2	3
20180423013547	2018-04-23	01:35:24.030	44.6992	9.7093	26.2	2.3	ML	141	144					A3	3
20180423014451	2018-04-23	01:44:07.820	44.6972	9.6987	27.4	2.0	ML	142	145					A3	3
20180423031602	2018-04-23	03:15:58.020	44.9107	11.6928	7.6	2.6	ML	36	37	16	FERS	2.9	MI10; MI05	A2	3
20180423031743	2018-04-23	03:17:34.350	44.9237	11.6973	7.1	2.5	ML	37	38					A3	3
20180423050712	2018-04-23	05:07:12.080	44.7860	12.0277	8.4	3.0	ML	47	47					A3	3
20180425010852	2018-04-25	01:08:16.480	43.0612	13.0378	8.1	3.5	ML	214	214					A3	3
20180425094939	2018-04-25	09:48:41.280	41.8785	14.8598	28.7	4.3	Mw	410	411					A3	3
20180429014219										3	CAVE	2.8	NDIM; MI10	B2	3
20180501051722	2018-05-01	05:16:58.200	43.2280	10.9312	7.4	3.6	ML	162	162					A3	3
20180503141909	2018-05-03	14:19:09.570	44.0502	11.7198	6.7	3.3	ML	66	67					A3	3
20180503184604	2018-05-03	18:46:04.650	44.0555	11.7137	7.4	3.6	ML	66	66					A3	3
20180503190330	2018-05-03	19:03:14.370	44.0548	11.7157	6.0	2.6	ML	66	66					A3	3
20180503235237	2018-05-03	23:52:21.630	44.0883	11.7303	5.0	2.6	ML	63	63					A3	3
20180504014239	2018-05-04	01:42:18.350	44.7730	10.6902	8.4	2.3	ML	65	66					A3	3
20180506020101	2018-05-06	02:00:59.060	44.8487	11.2432	6.3	2.0	ML	32	32	18	RAVA	3.8	CAVE; NDIM	A2	3
20180509214836	2018-05-09	21:48:01.940	46.3032	13.1048	9.1	3.6	ML	226	226					A3	3
20180511025742	2018-05-11	02:57:36.610	44.8552	11.2983	8.0	1.8	ML	30	31	11	RAVA	4.6	A307A; CAVE	A2	3
20180511162234	2018-05-11	16:22:27.700	44.7007	11.8632	7.4	2.3	ML	31	32	7	A308A	3.8	MI10 ; MI02	A2	3
20180519000151	2018-05-19	00:01:27.140	44.8682	9.6973	23.6	2.2	ML	144	146					A3	3
20180519013803	2018-05-19	01:37:44.710	44.8697	9.6927	22.7	2.7	ML	145	147					A3	3
20180519164121	2018-05-19	16:41:21.940	44.8233	9.6822	28.7	4.1	ML	145	148					A3	3
20180519165150	2018-05-19	16:51:06.830	44.8452	9.7052	23.1	2.6	ML	143	145					A3	3
20180519200642	2018-05-19	20:06:18.550	44.8387	9.7057	25.0	3.0	ML	143	145					A3	3
20180521034955	2018-05-21	03:49:32.660	45.5907	10.1948	6.7	2.9	ML	148	148					A3	3
20180521085008	2018-05-21	08:49:26.510	43.0822	13.0158	8.4	3.9	ML	211	211					A3	3
20180521220358	2018-05-21	22:03:55.640	44.7998	11.4538	8.8	1.9	ML	20	22	12	FERS	3.3	MI10; A307A	A2	3
20180522221000	2018-05-22	22:09:54.890	44.2422	11.6748	10.0	1.9	ML	45	46	3	BRIS	2.9	IMOL; MTRZ	A2	3
20180606001440	2018-06-06	00:13:57.140	44.8942	9.6798	20.1	2.0	ML	147	148					A3	3
20180609215940	2018-06-09	21:59:24.920	44.2177	11.2783	9.8	1.4	ML	48	49	3	ZCCA	6.3	BRIS; MI08	A2	3

Table 2 - continued.

Event ID	Origin Date	Origin Time	Latitude	Longitude	h [km]	M	M Type	D [km]	R [km]	NSP	SN1	SP1	SN2-3	ET	EC
20180625051917	2018-06-25	05:14:47.260	36.7348	21.4058	19.1	5.3	Mw	1211	1211					A3	3
20180625115046	2018-06-25	11:50:30.480	44.1343	10.9978	9.7	2.7	ML	67	68					A3	3
20180701073232	2018-07-01	07:32:16.680	44.1803	10.5480	14.2	3.6	ML	90	91					A3	3
20180701073905	2018-07-01	07:38:47.330	44.2052	10.5597	11.8	2.8	ML	87	88					A3	3
20180701081026	2018-07-01	08:10:07.770	44.2017	10.5725	14.4	2.8	ML	87	88					A3	3
20180701105950	2018-07-01	10:59:26.560	44.2105	10.5613	12.7	2.1	ML	87	88					A3	3
20180701154558	2018-07-01	15:45:40.750	44.1960	10.5505	11.1	2.4	ML	89	89					A3	3
20180701180838	2018-07-01	18:08:21.570	44.1918	10.5587	14.5	2.6	ML	89	89					A3	3
20180701190251	2018-07-01	19:02:34.630	44.1868	10.5497	17.9	2.9	ML	89	91					A3	3
20180701234133	2018-07-01	23:41:17.920	44.1737	10.5402	18.1	3.0	ML	91	92					A3	3
20180702124052	2018-07-02	12:40:29.550	44.4053	12.3622	31.8	2.5	ML	73	80					A3	3
20180704090247	2018-07-04	09:01:08.979	41.4475	19.5630	14.6	5.1	Mb	745	746					A3	3
20180708125044	2018-07-08	12:50:11.320	44.5110	10.2097	22.2	1.7	ML	102	105					A3	3
20180722041630	2018-07-22	04:16:04.060	44.8187	10.7680	31.7	2.0	ML	61	69					A3	3
20180722101242	2018-07-22	10:07:26.400	34.4500	46.1300	10.0	5.8	Mw	3154	3154					A3	3
20180726012702	2018-07-26	01:26:46.910	44.7638	12.6593	33.3	2.0	ML	94	100					A3	3
20180811032800	2018-08-11	03:26:58.860	46.3357	13.0517	8.9	3.1	ML	226	226					A3	3
20180811033115	2018-08-11	03:30:38.780	46.3387	13.0357	10.3	3.6	Mw	226	226					A3	3
20180811154017	2018-08-11	15:38:35.573	41.5389	20.0513	18.2	5.2	Mb	776	776					A3	3
20180811232511										6	FERS	1.8	MI10; SERM	B2	3
20180812214401	2018-08-12	21:43:16.540	43.5678	12.1032	7.3	2.9	ML	127	127					A3	3
20180813200442										8	A308A	4.0	CMPO; MI10	B2	3
20180814214926	2018-08-14	21:48:30.980	41.8877	14.8407	19.2	4.6	Mw	408	408					A3	3
20180815092759	2018-08-15	09:27:22.730	45.7192	11.2443	12.6	2.3	ML	124	124					A3	3
20180816182002	2018-08-16	18:19:04.600	41.8742	14.8648	19.6	5.1	Mw	410	411					A3	3
20180816202331	2018-08-16	20:22:34.780	41.8728	14.8747	21.6	4.4	Mw	411	412					A3	3
20180818123141	2018-08-18	12:30:57.030	44.4633	9.8233	17.2	2.6	ML	133	135					A3	3
20180819003832	2018-08-19	00:19:38.750	-18.0773	-178.0660	574.2	8.1	Mwpd	16950	16961					A3	3
20180821003345	2018-08-21	00:33:45.610	44.7933	10.6638	8.1	3.7	Mw	68	69					A3	3
20180821010732	2018-08-21	01:07:06.780	44.7837	10.6580	5.5	2.3	ML	68	68					A3	3
20180821132609	2018-08-21	13:26:04.460	44.8587	11.4542	7.8	2.1	ML	26	28	4	FERS	2.6	MI10; A307A	A2	3
20180821214250	2018-08-21	21:31:41.289	10.6664	-62.8945	105.5	7.0	Mwpd	7953	7953					A3	3
20180830033411	2018-08-30	03:33:05.071	44.0402	16.5674	9.8	4.8	mb	409	410					A3	3
20180831130340	2018-08-31	13:03:17.670	43.9880	12.8890	33.3	3.5	Mw	132	136					A3	3
20180905014211	2018-09-05	01:41:59.070	44.3792	10.8117	26.1	2.3	ML	60	66					A3	3
20180906160814	2018-09-06	17:49:17.816	-18.4711	179.4420	647.7	7.7	Mwpd	16917	16930					A3	3
20180907203702	2018-09-07	20:35:04.000	43.4500	17.2500	8.0	4.0	ML	479	479					A3	3
20180909032309	2018-09-09	03:22:48.420	44.4157	10.7302	25.0	2.1	ML	65	69					A3	3
20180910063226	2018-09-10	06:32:00.100	44.9543	11.8273	31.1	1.8	ML	46	55					A3	3
20180911215755	2018-09-11	21:57:13.780	42.9475	13.1785	7.6	3.6	ML	231	231					A3	3
20180915031004	2018-09-15	03:09:14.000	43.8000	15.7500	10.0	4.2	ML	352	352					A3	3
20180915080123	2018-09-15	08:01:16.390	44.9040	11.2813	10.5	2.2	ML	35	37	3	RAVA	4.3	SERM; CAVE	A2	3
20180919095501	2018-09-19	09:54:41.480	44.2380	11.7837	20.1	2.7	ML	49	53					A3	3
20180923161730	2018-09-23	16:17:05.050	44.0490	11.8627	32.5	1.8	ML	70	76					A3	3
20180929070248										3	RAVA	4.1	CAVE; A307A	B2	3
20181001185200	2018-10-01	18:51:46.070	44.3143	11.0523	20.6	2.0	ML	49	53					A3	3
20181006233512	2018-10-06	23:34:56.620	44.2577	11.6638	18.9	1.5	ML	43	47	3	BRIS	3.3	IMOL; MI08	A2	3

Table 2 - continued.

Event ID	Origin Date	Origin Time	Latitude	Longitude	h [km]	M	M Type	D [km]	R [km]	NSP	SN1	SP1	SN2-3	ET	EC
20181007075100	2018-10-07	07:50:59.200	44.2622	11.6063	9.2	1.3	ML	41	42	2	BRIS	3.2	IMOL	A2	3
20181009005654	2018-10-09	00:56:37.500	44.2355	11.6742	19.4	1.9	ML	47	50	3	BRIS	3.3	IMOL; MI08	A2	3
20181013025126	2018-10-13	02:50:51.670	44.2742	12.6947	29.5	2.4	ML	103	106					A3	3
20181014042046	2018-10-14	04:20:29.360	44.1187	12.1155	7.5	2.1	ML	75	75					A3	3
20181014072322	2018-10-14	07:23:06.630	44.1262	12.1123	6.1	2.4	ML	74	74					A3	3
20181014143504	2018-10-14	14:34:38.130	44.1207	12.1082	6.3	2.0	ML	74	75					A3	3
20181014225721	2018-10-14	22:57:06.250	44.1193	12.1147	6.7	2.3	ML	75	75					A3	3
20181018032018	2018-10-18	03:20:13.790	44.8143	10.7493	9.4	2.2	ML	62	63					A3	3
20181022171604	2018-10-22	17:15:23.450	44.7015	9.7818	8.6	2.3	ML	136	136					A3	3
20181022174441	2018-10-22	17:44:22.180	43.9413	11.4878	5.8	2.4	ML	76	76					A3	3
20181025225713	2018-10-25	22:54:50.820	37.4924	20.5950	10.0	6.8	Mwp	1100	1100					A3	3
20181029115939										3	ZCCA	6.5	MI08; MI10	B2	3
20181030151435	2018-10-30	15:12:01.163	37.4889	20.5774	10.0	6.0	Mwp	1100	1100					A3	3
20181103093633	2018-11-03	09:36:24.320	44.4992	10.8632	27.6	2.7	ML	52	59					A3	3
20181108083518	2018-11-08	08:34:59.830	44.6127	10.1458	25.3	2.5	ML	107	109					A3	3
20181111072637	2018-11-11	07:26:31.860	44.2842	11.6740	24.5	1.7	ML	40	47					A3	3
20181113032538	2018-11-13	03:25:16.690	44.2712	11.1468	10.7	1.4	ML	48	49	3	ZCCA		MTRZ; BRIS	A2	3
20181115003832	2018-11-15	00:38:15.660	44.4715	10.3052	25.4	1.8	ML	95	99					A3	3
20181118124859	2018-11-18	12:48:46.400	44.0513	12.4858	36.8	4.2	ML	102	108					A3	3
20181118230738	2018-11-18	23:07:22.340	44.2663	11.6632	21.9	1.8	ML	42	47	3	BRIS	3.3	IMOL; MI08	A2	3
20181125064539	2018-11-25	06:45:10.970	43.9957	11.9100	26.0	1.6	ML	77	82					A3	3
20181125233222										3	CAVE	2.3	RAVA; NDIM	B2	3
20181126230444	2018-11-26	23:04:21.100	44.6317	9.5083	8.2	3.2	ML	157	157					A3	3
20181201222626	2018-12-01	22:26:22.040	44.7090	11.5440	6.1	0.6	ML	10	12	4	MI10	2.0	A307; MI05	B1	2
20181203000655	2018-12-03	00:06:47.740	44.2515	11.0478	19.6	3.2	ML	54	58					A3	3
20181203001114	2018-12-03	00:11:05.650	44.2458	11.0447	15.4	2.5	ML	55	57					A3	3
20181203013344	2018-12-03	01:33:37.110	44.2462	11.0387	14.8	2.3	ML	55	57					A3	3
20181204000820	2018-12-04	00:07:55.590	44.1077	10.7835	63.7	2.4	ML	80	103					A3	3
20181209202800	2018-12-09	20:27:21.850	45.5125	9.9053	9.9	2.6	ML	159	160					A3	3
20181212195121	2018-12-12	19:51:15.000	44.3397	11.8975	20.6	2.4	ML	45	50					A3	3
20181218040207	2018-12-18	04:02:00.490	44.8357	10.7273	7.7	2.3	ML	65	65					A3	3
20181219193721	2018-12-19	19:36:59.670	44.3317	10.8778	25.8	2.2	ML	58	64					A3	3
20181221090418	2018-12-21	09:04:02.210	44.6752	10.8382	31.0	2.0	ML	52	60					A3	3
20181221090824	2018-12-21	09:08:15.880	44.6832	10.8642	31.3	2.6	ML	50	59					A3	3
20181221175110	2018-12-21	17:50:45.080	43.5742	12.3357	8.0	3.5	ML	135	135					A3	3
20181221204127										5	IMOL	5.1	BRIS; MI08	B2	3
20181222091608	2018-12-22	09:15:53.340	44.9647	11.9817	19.1	2.3	ML	54	58					A3	3
20181223075250	2018-12-23	07:52:29.950	45.7617	11.7030	10.6	2.6	ML	128	128					A3	3
20181225222934	2018-12-25	22:29:20.250	44.2818	11.6202	41.5	1.3	ML	40	57					A3	3
20181226145348	2018-12-26	14:53:39.500	44.2710	11.4407	25.3	1.8	ML	40	47	3	MTRZ	3.0	BRIS; IMOL	A2	3
20181229185648	2018-12-29	18:56:43.230	44.2695	11.4402	22.7	2.7	ML	40	46	3	MTRZ	4.0	BRIS; IMOL	A2	3
20190101183836	2019-01-01	18:37:46.960	41.8777	13.5488	16.5	4.2	ML	349	349					A3	3
20190101212910	2019-01-01	21:28:35.320	43.8732	12.0298	6.8	1.9	ML	94	94					A3	3
20190102070116										3	MI10	2.2	MI02; MI08	B0	0
20190104192938	2019-01-04	19:23:39.300	42.2000	19.8200	10.0	4.7	ML	725	725					A3	3
20190106234904	2019-01-06	23:48:37.730	44.1255	13.1588	26.3	2.3	ML	144	146					A3	3
20190107185723	2019-01-07	18:57:07.660	44.2637	11.0302	16.6	1.9	ML	54	57					A3	3

Table 2 - continued.

Event ID	Origin Date	Origin Time	Latitude	Longitude	h [km]	M	M Type	D [km]	R [km]	NSP	SN1	SP1	SN2-3	ET	EC
20190108010820	2019-01-08	01:08:18.250	44.8242	11.4438	0.5	0.6	ML	23	23	5	MI10	2.3	MI05; MI01	B1	3
20190111014813	2019-01-11	01:48:10.640	44.7517	11.7137	4.6	0.9	ML	23	23	5	MI10	2.3	MI02; MI01	B1	3
20190114230405	2019-01-14	23:03:57.020	44.3467	12.2857	20.6	4.6	ML	70	73					A3	3
20190114231810	2019-01-14	23:17:48.020	44.3580	12.2377	24.5	1.9	ML	66	71					A3	3
20190114232918	2019-01-14	23:29:07.990	44.3322	12.2932	22.0	3.0	ML	72	75					A3	3
20190115004554	2019-01-15	00:45:40.000	44.4750	12.2875	11.4	2.2	ML	65	66					A3	3
20190115013019										3	BRIS	4.6	MI10; MI08	B2	3
20190115034433	2019-01-15	03:44:13.900	44.3718	12.1487	20.5	2.0	ML	59	63					A3	3
20190115035753	2019-01-15	03:57:28.720	44.4052	12.0988	22.9	2.0	ML	54	59					A3	3
20190117071621	2019-01-17	07:15:56.840	44.4042	12.1393	21.0	2.2	ML	57	61					A3	3
20190119024205										7	A308A	6.6	BRIS; MI08	B2	3
20190119123718	2019-01-19	12:36:49.520	44.1292	12.2463	6.6	1.5	ML	82	82					A3	3
20190120211815	2019-01-20	21:17:50.530	44.4293	12.2318	9.5	1.7	ML	63	64					A3	3
20190120232429	2019-01-20	23:24:17.160	44.4228	12.1927	17.9	1.9	ML	60	63					A3	3
20190121184031	2019-01-21	18:40:26.980	44.8370	11.4625	7.3	1.5	ML	24	25	9	MI10	2.5	A307A; MI05	B1	3
20190122203053	2019-01-22	20:30:35.810	44.1652	10.6243	7.9	2.4	ML	86	86					A3	3
20190123201741	2019-01-23	20:17:31.070	44.3295	11.3765	32.5	1.8	ML	34	47	4	MI08	4.9	MI03; MI02	B1	3
20190125210209	2019-01-25	21:02:03.700	44.3350	11.8887	22.3	2.8	ML	45	50	16	IMOL	5.7	BRIS; A308A	A3	3
20190126091810										1	MI10	5.6		B0	0
20190126151918	2019-01-26	15:19:11.850	44.6672	11.9198	9.4	2.4	ML	35	36	13	A308A	3.3	CMPO; MI10	A2	3
20190201221820	2019-02-01	22:18:09.070	43.9970	11.6558	6.3	3.3	ML	71	71					A3	3
20190202164043										2	MTRZ	4.6	MI08	B2	3
20190204222519										4	A308A	5.7	BRIS; MI08	B2	3
20190205021935	2019-02-05	02:19:32.630	44.4952	10.0953	21.9	2.8	ML	112	114					A3	3
20190205114818	2019-02-05	11:47:51.690	44.4375	12.1860	31.0	2.2	ML	59	67					A3	3
20190206233341	2019-02-06	23:33:23.540	44.0060	11.6678	6.3	2.1	ML	70	70					A3	3
20190208040649	2019-02-08	04:06:43.340	44.2783	11.8767	24.6	2.2	ML	49	55					A3	3
20190215043932	2019-02-15	04:39:18.450	44.3062	10.6810	6.8	2.2	ML	73	74					A3	3
20190217145416	2019-02-17	14:35:55.000	-3.3500	152.2300	359.0	6.2	Mwp	14045	14049					A3	3
20190218182351	2019-02-18	18:23:40.890	44.7437	10.6502	28.0	2.4	ML	69	73					A3	3
20190301030640	2019-03-03	03:06:26.410	44.2262	11.2008	19.3	1.4	ML	50	53					A3	3
20190303034943	2019-03-03	03:49:33.130	44.4607	11.3243	43.3	1.5	ML	22	49	7	MI06	5.4	MI01; MI03	B1	3
20190307020720	2019-03-07	02:06:59.770	43.8088	11.9600	9.7	2.3	ML	98	99					A3	3
20190307024319	2019-03-07	02:43:07.980	44.1708	11.2378	10.8	1.6	ML	54	55					A3	3
20190308165504	2019-03-08	16:55:01.910	44.8417	11.3947	4.1	2.0	ML	25	25	9	A307A	2.8	MI05; MI10	B1	3
20190313142225	2019-03-13	14:22:18.680	44.9075	11.2398	9.4	2.5	ML	37	38	9	RAVA	5.1	SERM; CAVE	A2	3
20190316061027	2019-03-16	06:10:23.580	44.3745	11.6153	34.6	3.0	ML	29	45	16	IMOL	6.2	BRIS; MTRZ	A2	3
20190321214307	2019-03-21	21:42:47.170	44.4857	9.8368	7.7	3.0	ML	132	132					A3	3
20190322215920	2019-03-22	21:59:00.120	44.1115	12.0503	7.5	2.2	ML	72	72					A3	3
20190322220838	2019-03-22	22:08:12.750	44.1110	12.0475	7.2	2.0	ML	72	72					A3	3
20190322222205	2019-03-22	22:21:38.240	44.1293	12.0358	8.5	1.7	ML	70	71					A3	3
20190322222415	2019-03-22	22:23:57.490	44.1253	12.0253	9.4	2.1	ML	70	71					A3	3
20190322222635										7	FAEN	4.8	BRIS; IMOL	B2	3
20190322222646	2019-03-22	22:27:11.640	44.1111	12.0455	5.8	1.8	ML	72	72					A3	3
20190322222856	2019-03-22	22:28:38.020	44.1023	12.0492	4.9	2.3	ML	73	73					A3	3
20190322223108	2019-03-22	22:30:55.820	44.1152	12.0393	8.2	2.6	ML	71	72					A3	3
20190323120405	2019-03-23	12:03:37.320	44.0953	11.0207	9.9	1.8	ML	70	70					A3	3

earthquakes by using labels A and B to denote events included and not-included in the ISN bulletin, respectively. Earthquakes labelled A were further subdivided as earthquakes of Event-Type A0, A1, A2 or A3, based on their distance from the surface projection of the centre of the reservoir and, for the cases A1 and A2, based on the station which recorded the first direct P-wave arrival (see Table 2 caption). Earthquakes not included in the ISN bulletin, were instead subdivided in events of Event-Type B0, B1, and B2, based on the station which recorded the first direct P-wave arrival and, for the cases B0 and B1, based on the number of the observed direct P-wave arrivals (see Table 2 caption). The Event-Type parameter represents an intermediate classification of the events, useful to produce the final outcome of the ILG experimentation, the parameter Event-Class, which takes the values 0, 1, 2 or 3 according to event location (see Table 2 caption). In particular, the Event-Class 1 and 3 denote seismic events located within the IDD and outside the EDD, respectively.

The above described classification scheme allowed us to proceed with the re-location solely for the earthquakes with Event-Type A0, A1, and B1. Indeed, seismic events with Event-Type A2, A3, and B2 were considered located outside the EDD. In the period 1 January 2018 - 31 March 2019, we observed 35, 163, and 17 events with Event-Type A2, A3, and B2, respectively, for a total number of 215 earthquakes located outside the EDD (Event-Class 3). Table 2 also includes 7 events with Event-Type B1 and 2 events with Event-Type B0. Earthquakes labelled B1 were localised by using Hypoellipse (Lahr, 1979) through the software package SacPicker (Spallarossa *et al*., 2011), which also allows us for local magnitude computation. For event location, we adopted the 1D velocity model reported in Table 3. The model was provided by the Concessionaire, and it was also used to localise the events included in the seismicity bulletin of the period 1979-2015. Thinking of a comparison with this bulletin, as a first stage of application of the ILG, we decided to adopt the same model to locate the recent earthquakes recorded by the MISN. However, despite the low seismicity characterising the EDD, the above described MISN implementation should allow a future improvement of the location model.

Table 3 - 1D velocity model used for earthquakes location: Δh is the layer thickness and h is the depth of the top of each layer.

Δh (km)	h (km)	Vp (km/s)	Vp/Vs
0.2	0.0	1.7	1.73
1.3	0.2	2.1	1.73
4.0	1.5	2.7	1.73
5.5	5.5	5.0	1.73
13.0	11.0	6.3	1.73
half-space	24.0	8.2	1.73

Earthquakes with Event-Type B1 recorded during the analysed period have hypocentral distances, R, ranging between 12 and 49 km. R is measured with respect to the surface projection of the centre of the reservoir. For these events, magnitudes range between 0.6 and 2.0 and, generally, the Event-Class is 3. 5 of them are located in the Ferrara Fold system at depths less than 8.0 km. The remaining, characterised by M_L = 1.5 and 1.8, have been localised in the Apennines at depths

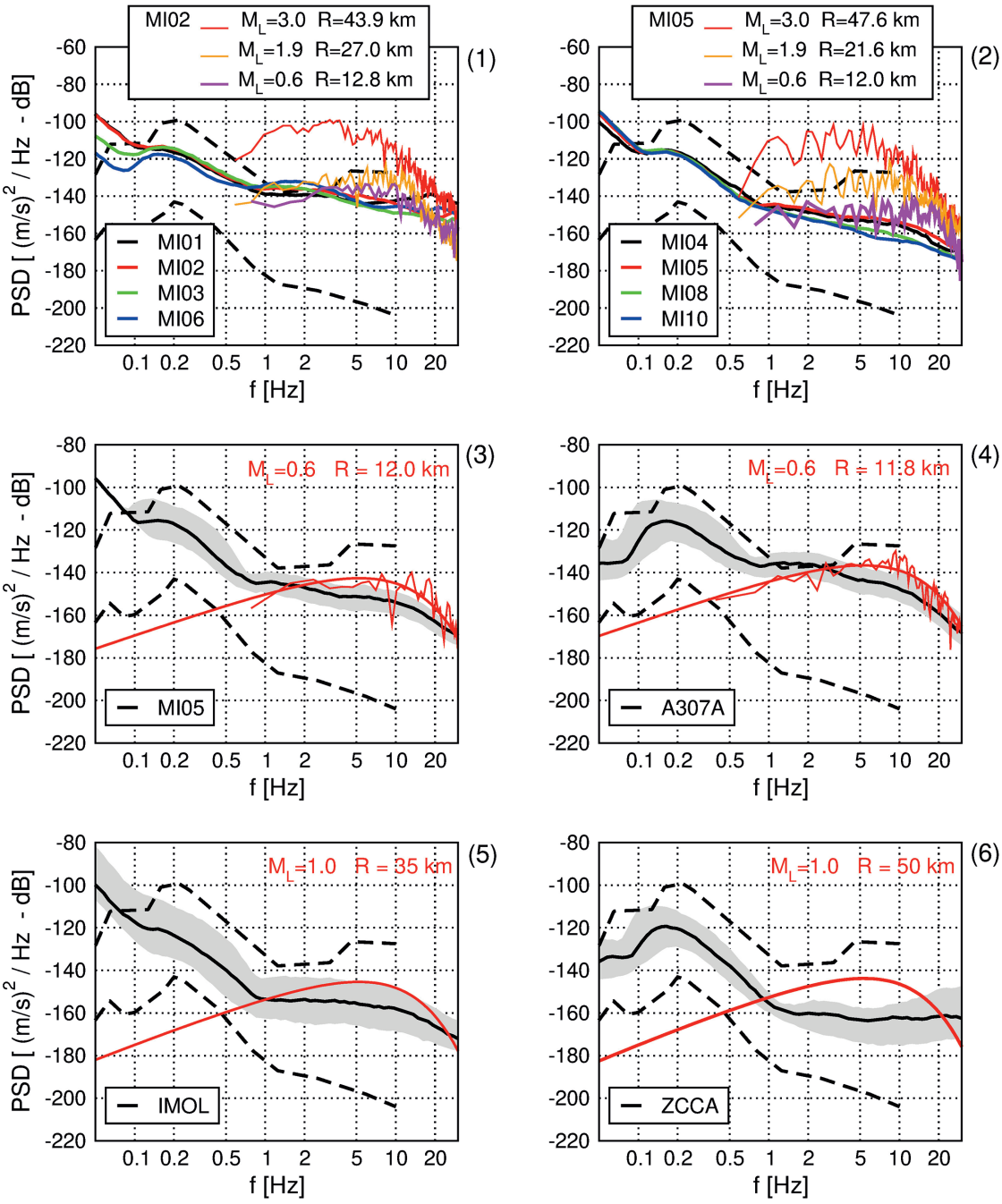

Fig. 10 - Validation of results: examples of simulated and recorded power spectra. Panel 1: mean horizontal component of velocity power spectra recorded at surface station MI02. Panel 2: mean horizontal component of velocity power spectra recorded at borehole station MI05. Power spectra of the recorded events, having magnitudes 0.6, 1.9, and 3.0, are compared with the median PDF of the ambient seismic noise, recorded with surface and borehole stations (panels 1 and 2, respectively). Panels 3 and 4: mean horizontal component of recorded and simulated power spectra for the M_L 0.6 event localised in the IDD. For the borehole station MI05 (panel 3) and the surface station A307A (panel 4) the earthquake power spectra are compared with the corresponding PDF of the observed ambient seismic noise. Panels 5 and 6: power spectra of a M_L 1.0 event hypothetically located at the centre of the reservoir, and simulated at stations IMOL (Po Plain - borehole) and ZCCA (Apennines - surface). Simulated PSD are compared with the corresponding PDF of observed ambient seismic noise. Dashed lines: NHNM and NLNM curves of Peterson (1993).

greater than 30 km. Only one of these earthquakes (characterised by M_L = 0.6 and R = 12 km), is located within the monitored crustal volume, near the border of the EDD.

As previously mentioned, we used the earthquakes recorded in this period to validate location thresholds estimated through detection analysis. We consider this kind of analysis a preliminary validation of the results obtained for the area of the reservoir. Indeed, due to the low seismicity levels of this area, both parameter calibration and validation of results should be continuously updated in order to increase the reliability of the estimated thresholds. Fig. 10 shows some examples of simulated and recorded power spectra that may prove useful for this purpose. The upper panels, showing the results obtained with surface and borehole stations, highlight the capability of the MISN to reliably detect seismic events occurring in the area, in the range of magnitudes 0.6-3.0. Indeed, the smallest earthquake is well recorded over the median value of the PDF of ambient seismic noise with both surface and borehole stations. On the other hand, the point source model employed in this study clearly fits the major event, also as regards borehole station MI05, whose spectrum is affected by the destructive interference of up-going and down-going waves. Central panels show recorded and simulated power spectra for the M_L 0.6 event localised in the IDD. The earthquake was detected near the limit of the detection threshold with both a surface and a borehole station. Finally, lower panels show the simulated power spectra for a M_L 1.0 event hypothetically located at the centre of the reservoir. Simulations highlight that, due to the favourable noise conditions characterising both surface stations installed in the Apennines and borehole stations installed in the Po Plain, these small events can be localised by the ISN. Therefore, location maps obtained with configuration C1, as those shown in Fig. 7, are produced by considering at least 4 stations able to detect this event (namely ZCCA, IMOL, MTRZ, and FIU).

6. Conclusions

The MISN is installed in a region characterised by very high levels of ambient seismic noise, which reach values up to 10 dB over the NHNM curve of Peterson (1993) in the hours of the most intense anthropic activity. This can negatively affect the detection capability of surface microseismic networks, even if they are equipped with at least some borehole sensors (100-200 m depth). Detection analysis of the MISN, carried out in this work for different configurations of the network, highlight the following points:

1) noise measurements, carried out during at least one year monitoring confirm both the high level and the high variability of ambient seismic noise, with differences between high- and low-noise conditions up to 20-25 dB;
2) borehole stations, installed in the Po Plain at shallow depths (100-150 m), show mean levels of ambient seismic noise, comparable with noise levels recorded at the surface by ISN stations installed in the Apennines;
3) average levels of noise recorded with borehole sensors are consistent with a general noise reduction with depth of about 0.1 dB/m. Indeed, borehole stations of the MISN show ambient seismic noise levels ranging from 10 to 20 dB less than corresponding levels observed at the surface;
4) detection analysis can be carried out by comparing the power spectrum of hypothetical earthquakes located in a crustal volume that includes the reservoir with the PSD of the

recorded ambient seismic noise, at each station-site. In this work, we model the hypothesised earthquakes as point sources located within the EDD, and compute M_L magnitude location thresholds for different configurations of the MISN by considering a minimum number of stations for earthquake detection equal to 4. Seismic events recorded by the MISN in the period 1 January 2018 - 31 March 2019, were used to improve the simulation parameters calibration with respect to detection analysis performed before the experimentation phase of the ILG. Detection analysis is particularly relevant for the IDD, the crustal volume of 11×11×5 km^3 centred on the reservoir, within which we should ensure the highest network performance;

5) before the experimentation phase of the ILG, the microseismic network managed by the Concessionaire, allowed obtaining at the bottom of the IDD, mean M_L location thresholds equal to 0.2, 0.8, and 1.4, in noise conditions corresponding to the 10th, 50th, and 90th percentile of the observed PDF of ambient seismic noise. In the same noise conditions, corresponding thresholds obtained with the stations of the ISN are: 0.6, 1.0, and 1.5, respectively. By integrating the microseismic network with ISN stations, the above mentioned thresholds become: 0.2, 0.8, and 1.2, respectively;
6) the installation of one more surface station and three more borehole stations within the EDD, enables improving the network performance by complying with the monitoring requirements prescribed by the ILG. Indeed, the present configuration of the MISN, allows obtaining at the bottom of the IDD, mean M_L location thresholds equal to 0.0, 0.5, and 1.0, in noise conditions corresponding to the 10th, 50th, and 90th percentile of the observed PDF of ambient seismic noise. At the bottom of the EDD, the corresponding thresholds are 0.4, 0.8, and 1.2;
7) in the period 1 January 2018 - 31 March 2019, the network recorded 224 seismic events, 198 of which are included in the catalogue of the ISN. All events recorded by the ISN, and 17 events recorded only by MISN stations, were located outside the EDD. 7 of the 9 remaining earthquakes recorded in this period, had enough observations of P and S arrivals in order to proceed with a reliable location. The localised events have M_L magnitudes ranging between 0.6 and 2.0, and are generally located outside the EDD. Only one of these earthquakes (characterised by M_L = 0.6 and R = 12 km), is located within the monitored crustal volume, near the border of the EDD;
8) detection analysis was validated with data recorded by the MISN during the analysed period. Comparisons of the PSD of seismic events recorded with both surface and boreholes stations of the microseismic network, highlight the capability of the MISN to reliably detect seismic events occurring in the area, in the range of magnitudes 0.6-3.0.

Due to the low seismicity of the area, detection analysis performed in this work should be further improved by comparing simulations with new recorded events. Before the experimental phase of the ILG, the MISN comprised 4 stations installed in the IDD, a relevant number with station spacing of 3.8 km. The present configuration of the MISN, without the need for new stations in the EDD, allows a maximum improvement of location thresholds of 0.2 unit magnitude with respect to the original configuration of the microseismic network. However, it also allows enlarging the areas where small events are confidently localisable. According to the guidelines issued by MiSE (ILG, 2014), even in the worst noise conditions observable in the area, the implemented configuration of the MISN, enables localising $M_L \geq 1.0$ events occurring in the whole IDD.

Acknowledgements. The authors wish to thank the "Comune di Minerbio" for the financial support under the grant "Sperimentazione ILG Minerbio" (grant number 0913.010). We also thank: Mise-DGS-UNMIG (Bologna), Regione Emilia Romagna and Stogit-Snam for their collaboration. The Editor in Chief and two anonymous reviewers are acknowledged for their constructive comments, which helped improve this article. This paper uses waveforms and data of the nationwide permanent seismological network (ISN), operated by the INGV. INGV data are available from FDSN Web Services (http://terremoti.ingv.it/webservices_and_software/). Furthermore, this paper uses third party waveform data (stations of Stogit microseismic network) that the authors do not have permission to distribute.

REFERENCES

AlpArray Seismic Network; 2015: *AlpArray Seismic Network (AASN) temporary component*. AlpArray Working Group, Other/Seismic Network, doi: 10.12686/alparray/z3_2015.

Amorese D.; 2007: *Applying a change-point detection method on frequency-magnitude distributions*. Bull. Seismol. Soc. Am., **97**, 1742-1749, doi: 10.1785/0120060181.

Anderson J.G. and Hough S.; 1984: *A model for the shape of Fourier amplitude spectrum of acceleration at high frequencies*. Bull. Seismol. Soc. Am., **74**, 1969-1994.

Boccaletti M., Corti G. and Martelli L.; 2011: *Recent and active tectonics of the external zone of the northern Apennines (Italy)*. Int. J. Earth Sci., **100**, 1331-1348, doi: 10.1007/s00531-010-0545-y.

Braun T., Cesca S., Kühn D., Martirosian-Janssen A. and Dahm T.; 2018: *Anthropogenic seismicity in Italy and its relation to tectonics: state of the art and perspectives*. Anthropocene, **21**, 80-94, doi: 10.1016/j.ancene.2018.02.001.

Brune J.N.; 1970: *Tectonic stress and the spectra of seismic shear waves from earthquakes*. J. Geophys. Res., **75**, 4997-5009, doi: 10.1029/JB075i026p04997.

Brune J.N.; 1971: *Correction*. J. Geophys. Res., **76**, 5002, doi: 10.1029/JB076i020p05002.

Burrato P., Ciucci F. and Valensise G.; 2003: *An inventory of river anomalies in the Po Plain, northern Italy: evidence for active blind thrust faulting*. Ann. Geophys., **46**, 865-882.

Cao A. and Gao S.; 2002: *Temporal variation of seismic b-values beneath northeastern Japan island arc*. Geophys. Res. Lett., **29**, 1334, doi: 10.1029/2001GL013775.

Carannante S., Argnani A., Massa M., D'Alema E., Lovati S., Moretti M., Cattaneo M. and Augliera P.; 2015: *The May 20 (M_W 6.1) and 29 (M_W 6.0), 2012, Emilia (Po Plain, northern Italy) earthquakes: new seismotectonic implications from subsurface geology and high-quality hypocenter location*. Tectonophys., **655**, 107-123, doi: 10.1016/j.tecto.2015.05.015.

Castro R.R., Pacor F., Puglia R., Ameri G., Letort J., Massa M. and Luzi L.; 2013: *The 2012 May 20 and 29, Emilia earthquakes (northern Italy) and the main aftershocks: S-wave attenuation, acceleration source functions and site effects*. Geophys. J. Int., **195**, 597-611, doi: 10.1093/gji/ggt245.

Cattaneo M., D'Alema E., Frapiccini M., Marzorati D. and Monachesi G.; 2011: *Acquisizione presso la sede di Ancona*. Miscellanea INGV, **10,** 124-127.

D'Alessandro A., Luzio D., D'Anna G. and Mangano G.; 2011: *Seismic network evaluation through simulation: an application to the Italian National Seismic Network*. Bull. Seismol. Soc. Am., **101**, 1213-1232, doi: 10.1785/01200066.

Edwards B., Kraft T., Cauzzi C., Kaestli P. and Wiemer S.; 2015: *Seismic monitoring and analysis of deep geothermal projects in St. Gallen and Basel, Switzerland*. Geophys. J. Int., **201**, 1020-1037.

Evernden J.F.; 1969: *Precision of epicenters obtained by small numbers of worldwide stations*. Bull. Seismol. Soc. Am., **59**, 1365-1398.

Franceschina G., Augliera P., Lovati S. and Massa M.; 2015: *Surface seismic monitoring of a natural gas storage reservoir in the Po Plain (northern Italy)*. Boll. Geof. Teor. Appl., **56**, 489-504.

Ghielmi M., Minervini M., Nini C., Rogledi S. and Rossi M.; 2013: *Late Miocene - Middle Pleistocene sequences in the Po Plain - northern Adriatic Sea (Italy): the stratigraphic record of modification phases affecting a complex foreland basin*. Mar. Pet. Geol., **42**, 50-81, doi: 10.1016/j.marpetgeo.2012.11.007.

Grigoli F., Cesca S., Priolo E., Rinaldi A.P., Clinton J.F., Stabile T.A., Dost B., Fernandez M.G., Wiemer S. and Dahm T.; 2017: *Current challenges in monitoring, discrimination, and management of induced seismicity related to underground industrial activities: an European perspective*. Rev. Geophys., **55**, 310-340, doi: 10.1002/2016RG000542.

Hanks T.C. and Boore D.M.; 1984: *Moment-magnitude relations in theory and practice*. J. Geophys. Res., **89**, 6229-6235, doi: 10.1029/JB089iB07p06229.

ISN; 2006: *INGV Seismological Data Centre, Rete Sismica Nazionale (RSN)*. Istituto Nazionale di Geofisica e Vulcanologia, Roma, Italy, doi: 10.13127/SD/X0FXNH7QFY.

Kraft T. and Deichmann N.; 2014: *High-precision relocation and focal mechanism of the injection-induced seismicity at the Basel EGS*. Geotherm., **52**, 59-73.

Kwiatek G. and Ben-Zion Y.; 2016: *Theoretical limits on detection and analysis of small earthquakes*. J. Geophys. Res., **121**, 5898-5916, doi: 10.1002/2016JB012908.

Lahr J.C.; 1979: *HYPOELLIPSE: a computer program for determining local earthquake hypocentral parameters, magnitude, and first-motion pattern*. U.S. Geological Survey, Reston, VA, USA, Open-File Report 79-431, 119 pp., doi: 10.3133/ofr79431.

Lay T. and Wallace T.C.; 1995: *Modern global seismology, 1st ed*. Elsevier, International Geophysics Series, Academic Press, San Diego, CA, USA, vol. 58, 521 pp.

McNamara D.E. and Buland R.P.; 2004: *Ambient noise levels in the continental United States*. Bull. Seismol. Soc. Am., **94**, 1517-1527, doi: 10.1785/012003001.

McNamara D.E. and Boaz R.I.; 2006: *PQLX: a software tool to evaluate seismic station performance*. Eos, Transactions, American Geophysical Union 87, Fall Meeting Abstract, S13B-0236.

McNamara D.E. and Boaz R.I.; 2011: *PQLX: a seismic data quality control system description, applications, and users-manual*. U.S. Geological Survey, Reston, VA, USA, Open-File Report 2010-1292, 41 pp.

MiSE - DGS - UNMIG; 2014: *Guidelines for monitoring seismicity, ground deformation and pore pressure in subsurface industrial activities*, <unmig.mise.gov.it/images/docs/151_238.pdf>.

Morelli A., Augliera P., Braun T., Danesi S. and Zaccarelli L.; 2018: *Applicazione sperimentale degli indirizzi e linee guida del MiSE per il monitoraggio di sismicità e deformazioni antropogeniche del suolo*. In: Riassunti estesi delle comunicazioni, 37° Convegno Nazionale, Gruppo Nazionale di Geofisica della Terra Solida, Trieste, Italy, pp. 537-538.

Peterson J.R.; 1993: *Observation and modelling of seismic background noise*. U.S. Geological Survey, Reston, VA, USA, Technical Report 93-322, 94 pp., doi: 10.3133/ofr93322.

Priolo E., Romanelli M., Plasencia Linares M.P., Garbin M., Peruzza L., Romano M.A., Marotta P., Bernardi P., Moratto L., Zuliani D. and Fabris P.; 2015: *Seismic monitoring of an underground natural gas storage facility: the Collalto Seismic Network*. Seismol. Res. Lett., **86**, 109-123, doi: 10.1785/0220140087.

Schorlemmer D. and Woessner J.; 2008: *Probability of detecting an earthquake*. Bull. Seismol. Soc. Am., **98**, 2103-2117, doi: 10.1785/0120070105.

Schorlemmer D., Mele F. and Marzocchi W.; 2010: *A completeness analysis of the National Seismic Network of Italy*. J. Geophys. Res., **115**, B04308, doi: 10.1029/2008JB006097.

Spallarossa D., Ferretti G., Scafidi D. and Pasta M.; 2011: *Picking automatico nella rete sismica dell'Italia Nord-Occidentale (RSNI)*. Miscellanea INGV, **10**, 141-146.

Stabile T.A., Iannaccone G., Zollo A., Lomax A., Ferulano M.F., Vetri M.L.V. and Barzaghi L.P.; 2013: *A comprehensive approach for evaluating network performance in surface and borehole seismic monitoring*. Geophys. J. Int., **192**, 793-806, doi: 10.1093/gji/ggs049.

Tramelli A., Troise C., De Natale G. and Orazi M.; 2013: *A new method for optimization and testing of microseismic networks: an application to Campi Flegrei (southern Italy)*. Bull. Seismol. Soc. Am., **103**, 1679-1691.

Vassallo M., Festa G. and Bobbio A.; 2012: *Seismic ambient noise analysis in southern Italy*. Bull. Seismol. Soc. Am., **102**, 574-586.

Wiemer S. and Wyss M.; 2000: *Minimum magnitude of completeness in earthquake catalogs: examples from Alaska, the western United States and Japan*. Bull. Seismol. Soc. Am., **90**, 859-869.

Wilson M.P., Foulger G.R., Gluyas J.R., Davies R.J. and Julian B.R.; 2017: *HiQuake: the human-induced earthquake database*. Seismol. Res. Lett., **88**, 1560-1565, doi: 10.1785/0220170112.

Woessner J. and Wiemer S.; 2005: *Assessing the quality of earthquake catalogues: estimating the magnitude of completeness and its uncertainty*. Bull. Seismol. Soc. Am., **95**, 684-698, doi: 10.1785/0120040007.

Corresponding author: Simona Carannante
Istituto Nazionale di Geofisica e Vulcanologia, Sezione di Milano
Via Alfonso Corti 12, 20100 Milano, Italy
Phone: +39 02 23699254; e-mail: simona.carannante@ingv.it